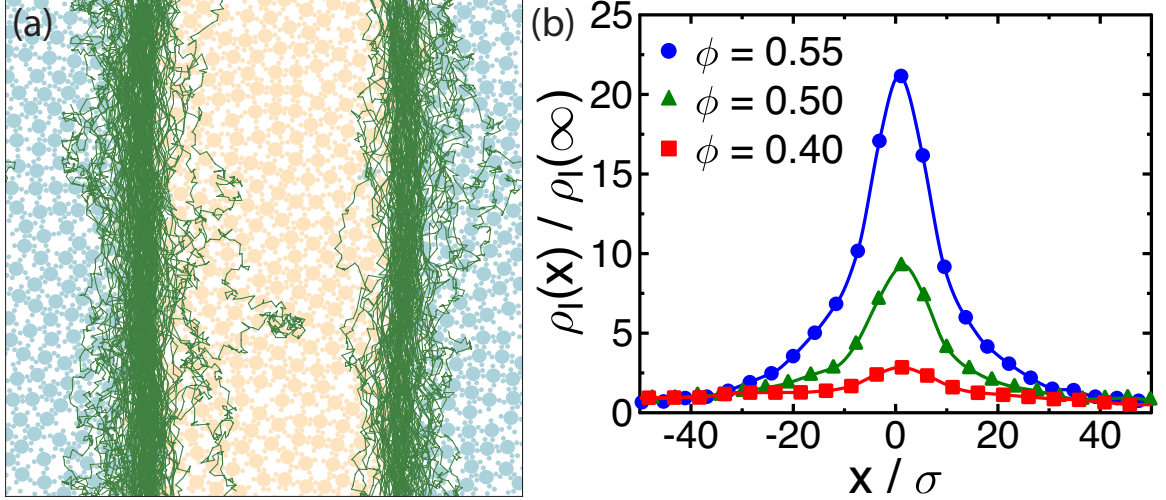**Figure 5.10** Vector plots show the short-time diffusion $\Delta\vec{x}(t)$ in systems of $N = 16384$ spinners at density of 0.6 where crystallization occurs. The system is driven by $\omega_0 = 1$ and 50:50 ratio. The observation time windows is $t = 100t_0$.

Figure 5.11 A system of 566 active spinners and 10 inactive spinners at density of 0.5. (a) Trajectories of inactive particles (green) at density of 0.5 and (b) their probability density close to an interface for different densities. The light blue spinners are driven by $\omega_0 = 1$.

and hard interaction as a spinner, but is not subject to a rotational driving torque. From their trajectories, Fig. 5.11(a), we observe that inactive particles diffuse to the interface and get dragged along the interface by the current of the active spinners. This observation is confirmed by the density of inactive particles as a function of the distance x to the interface, $\rho_I(x)$, relative to their density in the bulk, $\rho_I(\infty)$, which is strongly peaked at the interface, Fig. 5.11(b). The preference of inactive particles to sit at the moving interface increases with density and could be utilized for collective transport at mesoscopic scales.

5.6   Discussion

The phase separation of rotationally driven active particles is realizable in experiment provided the particles are permanently assigned a rotation direction while being free to move translationally and collide with one another. Applying torques to photo-sensitive spinners through optical trapping is one promising route [120, 121] and may even be possible on the colloidal scale where the dynamics can be observed through the microscope [119, 16]. In many situations, however, a restriction of the rotation direction is not possible. This is in particular the case for three-dimensional systems. Our observation of an emergent

preferential interaction between like rotating particles suggests a possible alignment [126] of the rotation axes in three dimensions. Whether actively rotated particles in three dimensions can indeed synchronize spontaneously into such a *nematic spinner phase* (alignment of the rotation axes) remains to be seen.

We also observe phase separation, rotating crystals, and collective transport at the interface with Brownian Dynamics simulations, where the inertial term is absent and the dynamics is dominated by viscous drag forces. Our choice of drag forces in the Langevin simulations induces particle motion comparable to Brownian dynamics [22]. This means inertia is not essential for the phenomena reported here and raises interesting questions about the presence or absence of local conservation of angular momentum. Finally, we note that the dynamics and interaction of actively rotated particles in a fluid can be influenced by hydrodynamic interactions [18, 118, 126], which are not taken into account here. We believe the tendency towards phase separation and synchronization is robust, if hydrodynamics induces an effective attraction between like rotating particles as in [122, 125]. Studying the phase behavior of externally driven or self-rotating (internally driven) spinners in a fluid environment remains an interesting open question.

Chapter 6

Self-Rotated Particles in Confinement

6.1 Introduction

This Chapter presents and discusses preliminary results of systems of driven spinners confined in a boundary. The research has been carried out in collaboration with Prof. Kyle Bishop's research group, an experimental group from the Pennsylvania State University. The research aims to 1) realize some of the results discovered in Chapter 5 and 2) explore a burgeoning research direction in confinement of active particles.

The effect of confinement on system dynamics and steady-state configurations has been studied in various contexts, from colloidal packing, liquid crystals, self-assembly of block copolymers, and microfluidic devices, to bacteria swarming and active matter. For example, colloids pack into novel polyhedral structures unlike minimum-potential clusters when confined in emulsion droplets [144] or pack more efficiently in sheared parallel plates [145]. In addition, confinement can induce a long-ranged pairwise-additive attraction between similarly charged colloidal spheres in equilibrium [146]. Colloidal crystals confined on a curved surface can self-heal their topological defects by a collective re-arrangement of the particles in response to the added interstitial [147]. Liquid crystals in confinement have been shown to impart ordered nanophases of surfactants on the boundary [148]. For polymeric systems, hard and soft confinement has been utilized to engineer copolymers into a variety of morphologies [149, 150, 151]. A single DNA experiences a crossover between two dynamical regimes as a result of changing its confined nanochannel width
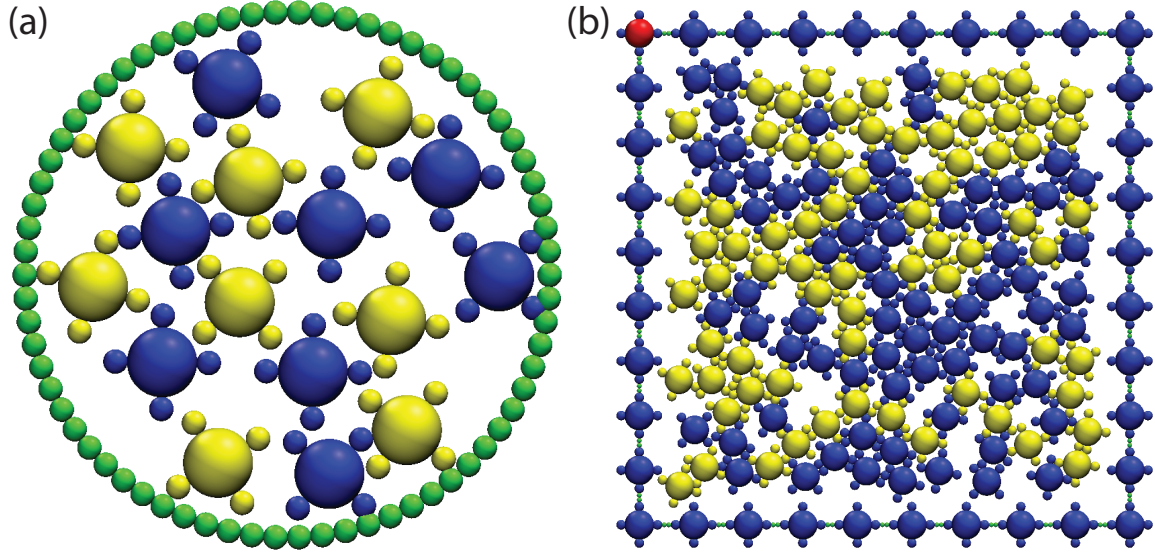
Figure 6.1 (a) An initial condition of 16 spinners of 50:50 mixture driven by $\omega_0 = 1$, in a rigid circular boundary at area density $\phi = 0.43$. (b) and of 142 interior spinners of 50:50 mixture driven by $\omega_0 = 1$, in a flexible boundary at $\phi = 0.5$. The boundary 36 spinners are connected by FENE springs (green) and are driven clockwise (blue). One spinner is colored red to track to motion of the boundary.

[152]. When confined within a 2D boundary, swimming bacteria exhibit interesting dynamics induced by hydrodynamic interactions, including concentration-dependent collective behavior [153, 154, 155] and preferential surface attachment [156]. Similarly, active rods confined in a boundary aggregate to the confining walls [65], exhibiting local ordering and swirling [116], and anomalous density fluctuation [17].

The research to date shows that confined systems can give rise to interesting, novel structures and properties not found in bulk systems. The studied systems have been limited mostly to hard surfaces serving as physical boundaries; however in a few examples, in which flexible boundaries [150] and interacting boundaries [148] were used, even richer physics have been discovered. In this Chapter, we investigate the behavior of self-rotated spinners confined by fixed and flexible boundaries. Our preliminary results show that fixed-boundary systems behave, in many ways, similar to the system in Chapter 5, and flexible-boundary systems give rise to new, rich phenomena.

Description	Symbol	Value	Unit
Radius of the Satellite Disks	σ	10.8	mm
Spinner mass	m	4.1	g
Spinner moment of inertia	I	2970	$g \cdot mm^2$
Spinner steady-state angular velocity	ω_0	2.3 (14.5)	Hz (rad/s)
Characteristic angular acceleration time scale	t_r	7.6	s
Rotational drag coefficient	$\gamma_r \approx I / t_r$	390	$g \cdot mm^2 \cdot s^{-1}$
Applied torque	$\tau^D \approx \omega_0 \gamma_r$	5.6	mN·mm

Figure 6.2 The experimental parameters of the spinners (Figure excerpted from a Bishop group's report).

6.2   Model and method

A typical confined system consists of a boundary and interior spinners. The interior spinners are modeled in the same way as in Chapter 5. A fixed boundary is a circular ring made of WCA beads that do not move (Fig. 6.1(a)). The flexible boundary is made of spinners that are linked by springs each spring consists of six WCA beads bonded by finitely extensible nonlinear elastic (FENE) springs (Fig. 6.1(b)). The force of a FENE spring relates to the distance between its ends, r, by

$$F_{FENE}(r) = \frac{rk}{1 - (\frac{r}{R_o})^2} \qquad (6.1)$$

where k is the stiffness and R_o is the maximum distance. If $R_o = \infty$, a FENE spring becomes a typical linear spring. The interactions between boundary spinners and interior spinners is WCA. A typical system is initialized in a square boundary with density of 0.5 (Fig. 6.1(b)). In all cases of flexible boundaries, the initial square boundary turns into a spherical one as its surface area is minimized and the boundary spinners can also be driven.

6.3 Systems of fixed boundaries

6.3.1 Experimental results

The experimental group realized the fixed boundary version of the system in Chapter 5 by using plastic discs floating on an air hockey table Fig. 6.3. The discs were fabricated by a 3D printer and rotated by blowing air through their holes in an azimuthal direction. The boundaries have been made "soft" by re-directing the air to blow horizontally from the boundaries; this is to avoid particles "frozen" into immobile states by sticking to the boundary. The physical parameters of a spinner are summarized in Table 6.2.

The rotation of a spinner is characterized by a dimensionless parameter, $\omega_0 t_r$, where $\omega_0 = \frac{\tau^D}{\gamma_r}$ is the terminal angular velocity and $t_r = \frac{I}{\gamma_r}$ is the time constant (eq. 5.1). This parameter also characterizes the importance of inertia relative to friction: for $\omega_0 t_r \ll 1$, friction dominates, and for $\omega_0 t_r \gg 1$, inertia dominates. For the experimental system, inertia dominates and $\omega_0 t_r = 109$. However, for the simulational system in Chapter 5, $\omega_0 t_r = 0.64$ and thus friction dominates. Nevertheless, we will show in subsequent sections that the characteristic behavior of the steady-state system is the same in both regimes.

At an intermediate density ($\phi = 0.43$), the demixing behavior was observed for even a small system of 16 particles. The system time evolution is summarized in the Fig. 6.4. The demixing is measured by an association coefficient, $c(t)$ that is defined as the ratio of the mean pairwise distance between like colors (white-white and blue-blue) to the mean pairwise distance between all unlike colors (white-blue). The system is initialized as a least associated (or most random) state with $c = 1.1$ and evolves to a nearly complete demixing with $c = 0.6$. Despite the small system size, the system still occasionally tends toward a more ordered, de-mixed state.

At higher density ($\phi = 0.45$), the system "locks": the particles cannot rotate because they become kinetically stuck to each other and the boundary. This locked state could be a result of 1) the fixed boundary and/or 2) not strong enough driving torque that allows
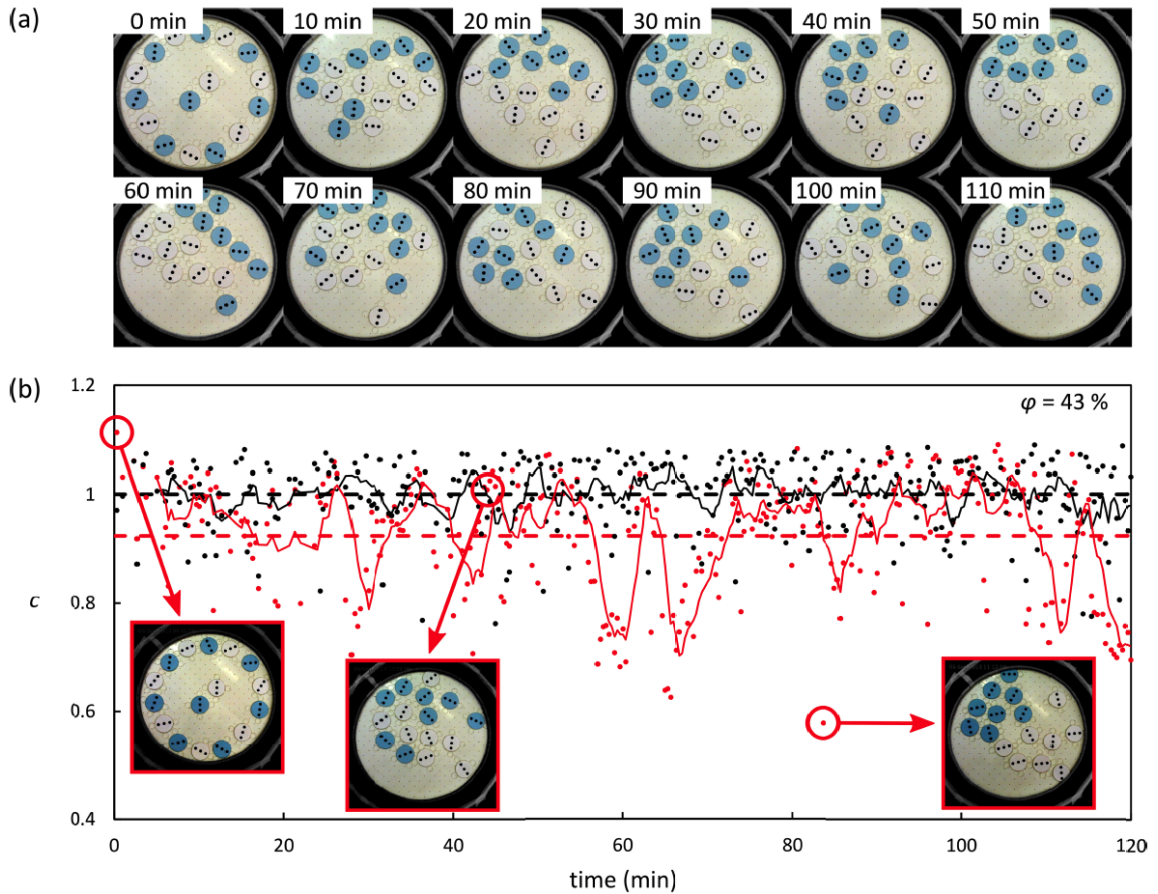
Figure 6.3 (a)Images of spinner system ($\phi = 0.43$) at regular intervals of 10 min. (b) Association coefficient $c(t)$ for the same system; the solid red line is a 120 s moving average and the dashed red line is the mean. Back points are from randomized disc assigments; as expected the mean of these data (dashed black line) is nearly 1. The insets show (from left to right) minimum association ($c = 1.1$), random association ($c = 1$) and maximum association ($c = 0.6$) (Figure excerpted from a Bishop group's report).

particles to unlock.

6.3.2 Simulational results

In order to 1) confirm the experimental results and 2) guide further experiments by exploring a broader parameter space, we perform simulations as described in Section 6.2.
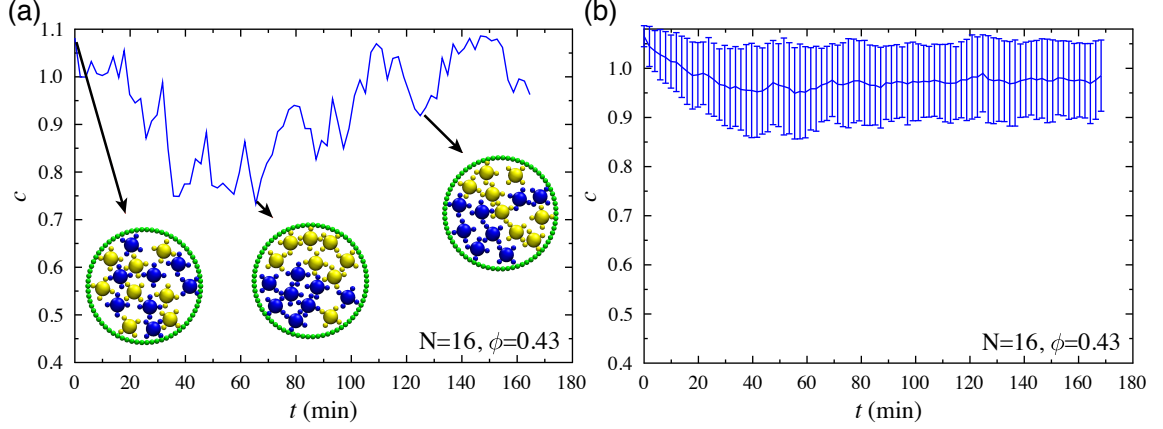
Figure 6.4 a) Simulation of 16 spinners at area density $\phi = 0.43$ and $\omega_0 t_r = 109$, which corresponds to the experimental system in Fig. 6.3. The plot shows the instantaneous association coefficient c every 1000 time units. The system tends toward demixing as it evolves from a minimally associated state ($c = 1.1$) to a strongly associated state ($c = 0.79$). We also observe random remixing and demixing in the system as indicated by large fluctuations in c as expected for a small, finite system. b) The average association coefficient and its standard deviation calculated over 100 runs of different random initial conditions. Other parameters are the same as in a). The system exhibits large fluctuations as one would expect from this small system size.

Mapping to experimental parameters

We employ the dimensionless parameter suggested by the Bishop group, $\omega_0 t_r = \frac{\tau^D I}{\gamma_r^2}$. For $\omega_0 t_r << 1$ friction dominates; for $\omega_0 t_r >> 1$ inertia dominates. We achieve the experimental value $\omega_0 t_r = 109$ by setting $\gamma_r = 1$ and $\tau^D = 1.7$ in our simulations. The moment of inertia is fixed by the geometry to $I = 64 m\sigma^2$ and the translational friction coefficient is kept at $\gamma_t = 1$. Equating the simulation time unit t_0 to the experiment time unit $t_r = \frac{I}{\gamma_r} = 64 t_0 = 7.6s$ gives $t_0 = 0.119s$.

Confirming experimental results

We performed simulations that map to the experiment in Fig. 6.3 and found good agreement in the results as shown in Fig. 6.4. Specifically, the system starting from a minimally associated state occasionally evolves toward strongly associated states. At area density $\phi = 0.48$ and 18 spinners, we observed a 'locked' state similar to that observed experimentally. In addition, we simulated 16 spinners at $\phi = 0.43$ and $\omega_0 t_r = 109$ with one particle

t=0	t=60 min	t=120 min
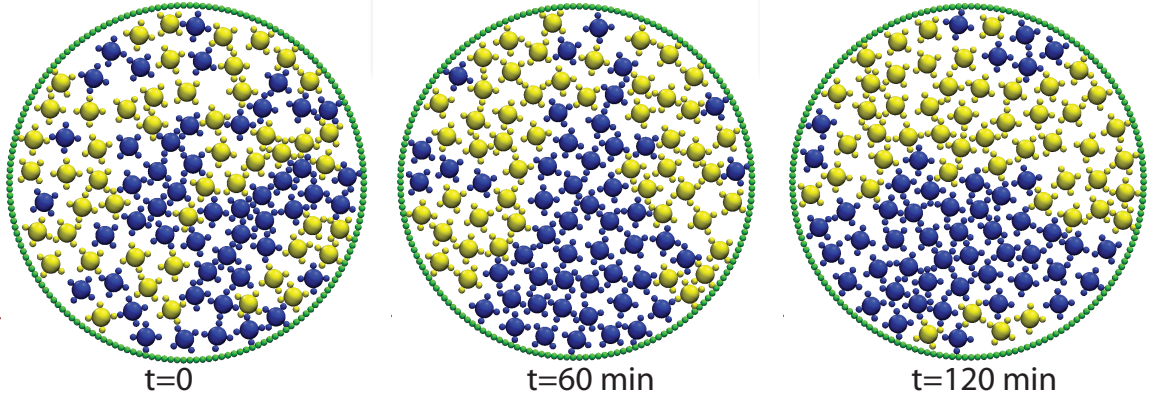
Figure 6.5 Simulation of 100 spinners at $\phi = 0.43$ and $\omega_0 t_r = 109$. The system exhibits a clear trend towards phase-separation.

immobilized. Part of the system became locked, while the remaining particles rotated at the optimal velocity ω_0. The immobilized particle acts as a nucleation site to immobilize others. We hypothesize that the system will become entirely locked,if there are more immobilized particles or if the system is at higher density; this hypothesis remains to be tested. The locked states represent a loss of ergodicity of the system and can be attributed to the fact the boundary is fixed.

Further simulations

Because of the influence of the fixed boundary, we expected the spinners to exhibit clearer phase-separation and even crystallization in a larger system. To confirm this expectation, we first simulated a system of 100 spinners at density $\phi = 0.43$. Indeed, demixing is much more pronounced as shown in Fig. 6.5.

However, at a system size of 100 particles, we did not observe crystallization even at density $\phi = 0.5$. Even when we increased the driving torque by a factor of 10 to $\omega_0 t_r = 1090$, still no crystallization was observed. Only when the system size is increased to 1000 particles, did we observe rotating crystals after 200 min in experimental time units.

Based on our preliminary simulations, we would recommend the following next steps for experiments to realize the phenomena reported in Chapter 5 and our PRL manuscript

t=20 min   t=200 min
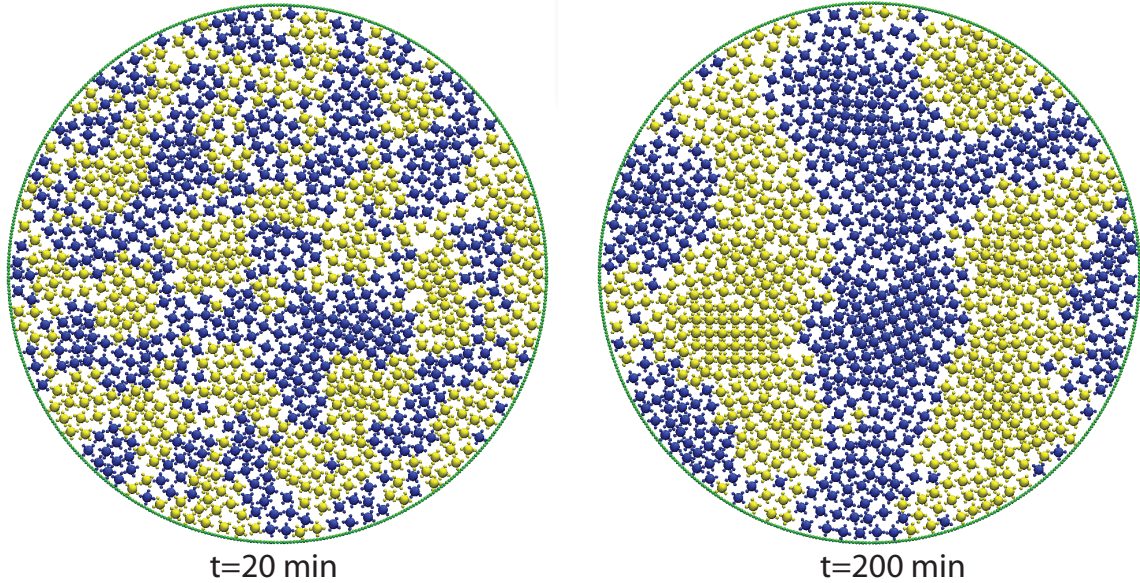
Figure 6.6   Simulation of 1000 spinners at $\phi = 0.5$ and $\omega_0 t_r = 109$. The system is initialized in a disordered state but exhibits phase-separation (left) and the formation of rotating crystals over time (right).

[23]:

1. Larger systems: We expect a stronger trend towards phase-separation at larger system size (on the order of 100 spinners). Even larger systems are needed to observe rotating crystals (in the order of 1000 spinners). As the system size increases, the influence of the fixed boundary on the system dynamics will decrease.

2. Stronger torques: A stronger driving torque would minimize the chance of the system getting stuck and speed up the dynamics at the same time.

3. We believe that the following directions might be interesting for experiment:

    (a) Add an inactive spinner that is not driven externally and compare its dynamics to the dynamics of active spinners. We observe the same super-diffusive behavior [23] that we observed at the boundary between phase-separated domains, around the edge of the crystal domains (Fig. 6.6) in these smaller systems; the spinners translate faster around the crystals. Studying dynamics of inactive particle would help elucidate the phenomenon and demonstrate potential applications in transport.

    (b) Study a one-component system. This allows the formation of rotating crystals at smaller system sizes and a better study of the crystal growth. Simulation work along these lines is being carried out by Spellings and Glotzer.
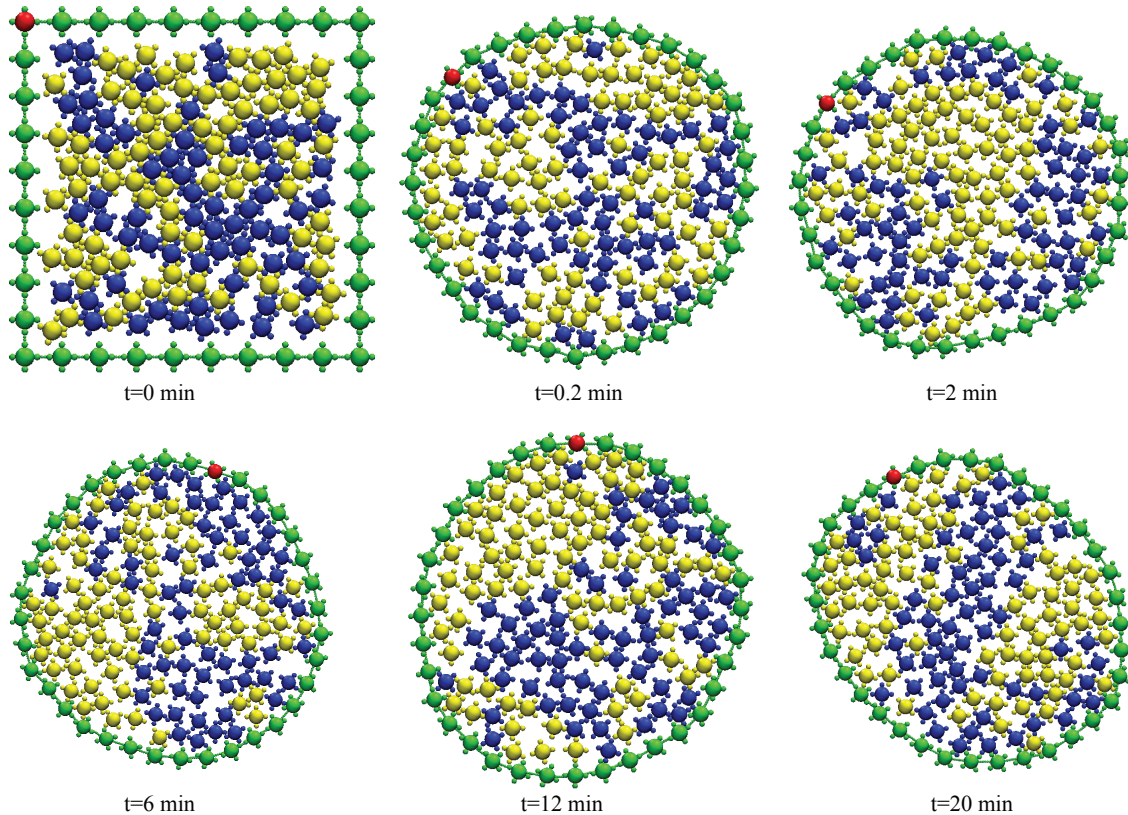
Figure 6.7 Time evolution of 142 spinners from 0 to $10000t_0$ or 20 minutes with a non-driven boundary initialized as in Fig. 6.1(b). The interior spinners are driven oppositely with CW:CCW ratio of 50:50 and by $\omega_0 = 1$. The interior spinners tend to demix into domains of like particles that seem to influence the system shape. The boundary rotates randomly (as opposed to exhibiting net rotation)

6.4 Systems of flexible boundaries

Because a flexible boundary is made of spinners connected by FENE springs, its spinners can be driven in similar manner to the interior ones. This ability can give one various ways of engineering interaction between a boundary and its interior and even with other confined systems. In the following sections, we will explore two main scenarios: non-driven and driven boundaries. Within the driven-boundary scenario, we explore cases of boundaries comprised of multiple spinner types (CW and CCW). The preliminary results show demixing and complex collective dynamics.

6.4.1 Non-driven boundaries

We simulated a system of 142 interior active spinners and a flexible boundary of 36 passive spinners, initialized at a density $\phi = 0.5$. The interior spinners are driven oppositely by a CW:CCW ratio of 50:50 while the boundary spinners are not driven but are free to rotate. As one would expect, the system demixes into domains of like spinners similar to the bulk and fixed-boundary systems (Fig. 6.7). The boundary rotates randomly and adopts different shapes depending on the demixing domains of the interior spinners. At $t = 0.2$ minutes, the interior spinners are still well mixed, and the boundary has a circular shape. But at $t = 20$, when the interior spinners demix into stripes, the boundary adopts an ellipsoidal shape. This ellipsoidal shape could be due to the decomposition of the spinners into stripes, breaking the circular symmetry, but this hypothesis requires testing.

6.4.2 Driven boundaries

**Active boundary of spinners rotating in a single direction**

In this case, the spinners of the boundary are driven clock-wise while those of the interior have a 50:50 ratio of CW:CCW. As a result, the interior spinners demix into annuli of like particles as shown in Fig. 6.8. The boundary rotates in the clockwise direction, the same as the direction of its individual spinners. This directional rotation of the boundary is due to the imbalanced numbers of driven spinners in the two opposite directions within the interior. Because the boundary spinners rotate, they push against interior spinners to move forward (Fig. 6.9) and thus, on average, the boundary will rotate in the direction of its majority spinner. As the boundary spinners and the spinners in contact with the boundary push against each other, they move in opposite directions. The inner spinners move about the annuli axis in the same direction. The demixing here is consistent with the finding in Chapter 5 that particles of the same type tend to aggregate.
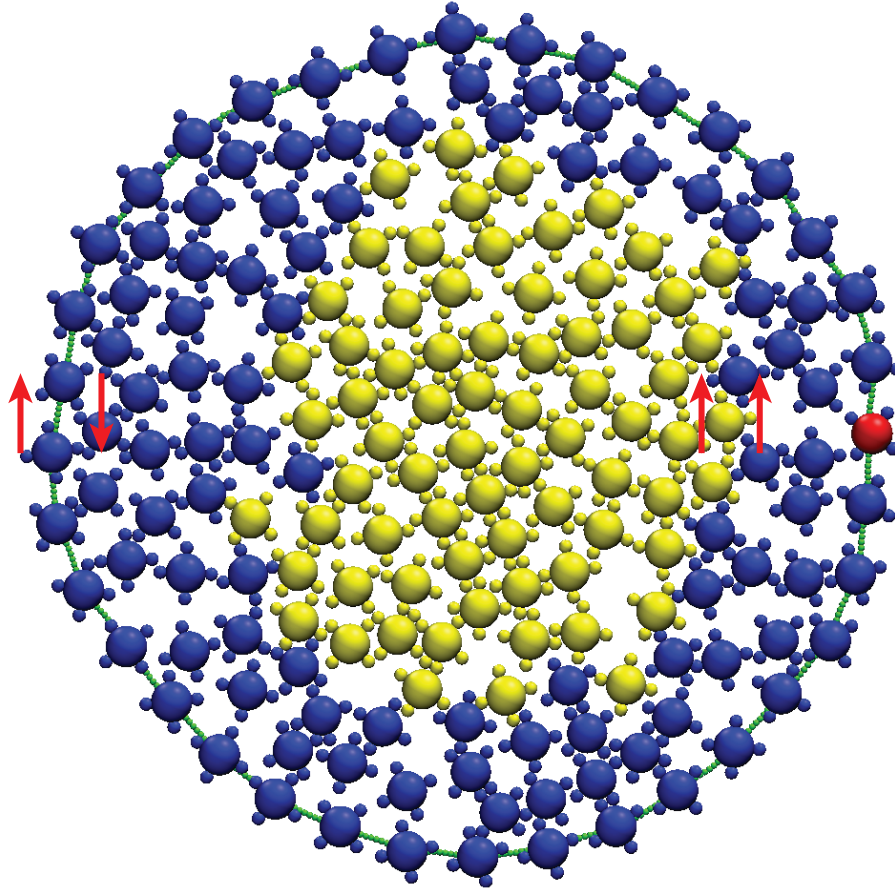
Figure 6.8 A snapshot of the system after 10000 time units. The boundary spinners are driven clockwise and the interior spinners driven with a 50:50 ratio of oppositely rotating spinners. For both types of spinner, $\omega_0 = 1$. The system phase separates into a core of (yellow) particles rotating counter-clockwise surrounded by spinners rotating oppositely. At the interface, the interior particles collectively translate in a counter-clockwise circular motion. The boundary rotates clockwise. The red arrows show translational motion directions.

Active boundary with 50:50 ratio of oppositely rotating spinners

In this case, the spinners of the boundary and the interior each are comprised of a 50:50 ratio of oppositely rotating spinners. The spinners demix into what we call a dynamical Janus [157] particle: like spinners occupy each half of the circular domain and are in contact with the part of the boundary with opposite spinners (Fig. 6.10). The spinners circulate in their domains in opposite directions. The formation of such configuration is supposed to be a result of the system avoiding frustration in the spinners collective motion. If the halves were to switch positions, collective motion would not possible because like particles push each
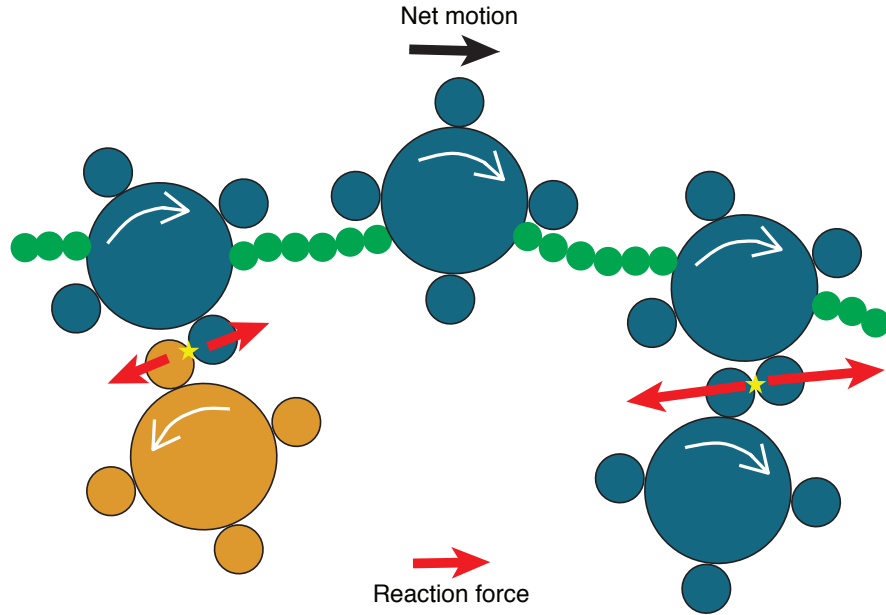
Figure 6.9   A schematic drawing of how a net boundary rotation arises from boundary spinners pushing against the interior particles. The reaction forces on the CW boundary spinners resulting from particle contacts dominantly point in the directions that cause the entire boundary to rotate CW.

other but are blocked by particles in the opposite half. The Janus configuration is not always perfect because some particles occasionally diffuse along the boundary to the opposite half and back to their own. When this diffusion happen, the boundary seems to rotate in one direction. In the perfect configuration, the boundary exhibits no directional rotation because the numbers of spinners are balanced.

Boundary of 67:33 ratio and interior spinners of 33:67 ratio of oppositely rotating spinners

In this case, the spinners of the boundary have a 67:33 ratio of CW to CCW of oppositely rotating spinners while the interior have the opposite ratio 33:67. This set-up is to test whether assigning the boundary and the interior spinners by opposite ratios would again yield a Janus-like configuration where particles at the surfaces are of opposite types. Indeed, we find Janus-like configurations, of course with imbalanced halves, in this case as well (Fig.6.11). We note, however, that the migration of the interior minority particles along the
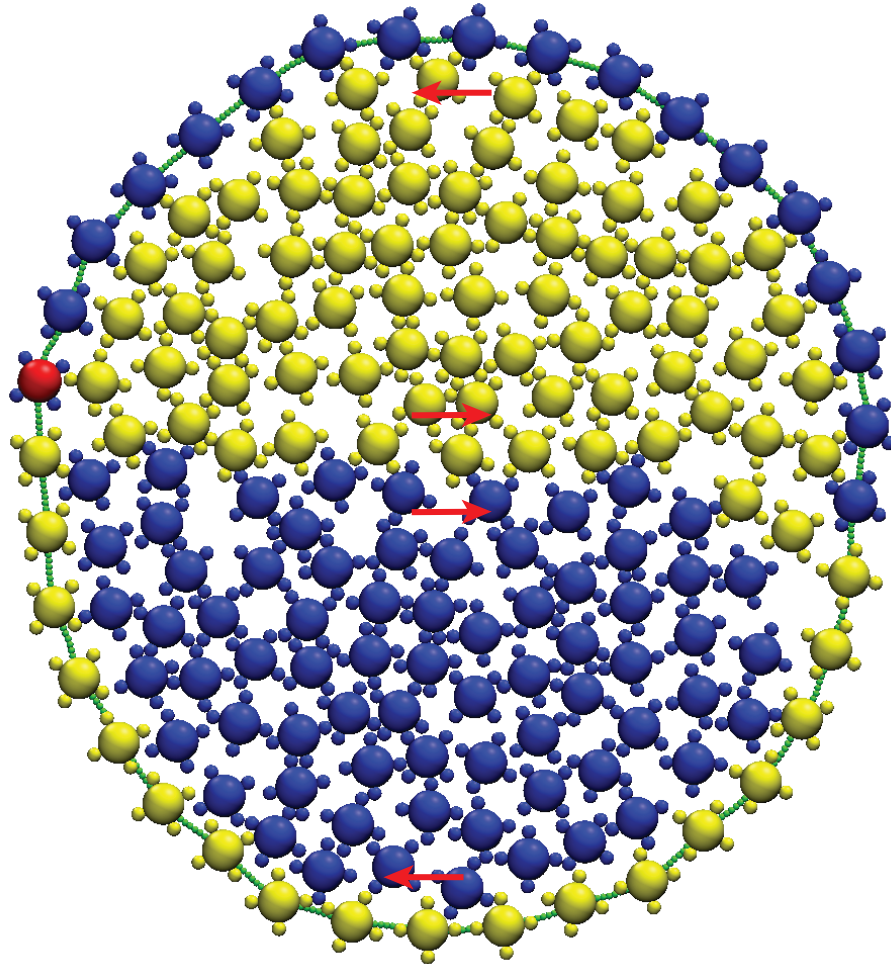
Figure 6.10 A snapshot of the system after 5000 t_0. The boundary and interior spinners each contain a 50:50 ratio of active spinners driven in opposite directions. The interior spinners separate into a dynamical Janus-like particle. Each domain of like particles are in contact with the oppositely-drive boundary. Translational motion of the interior spinners is shown by the red arrows. The spinners form two oppositely vortices, while the boundary does not exhibit any net rotation. The system does not always maintain a perfect Janus-like shape as a few spinners occasionally diffuse into the opposite domain at the boundary and translate along the it.
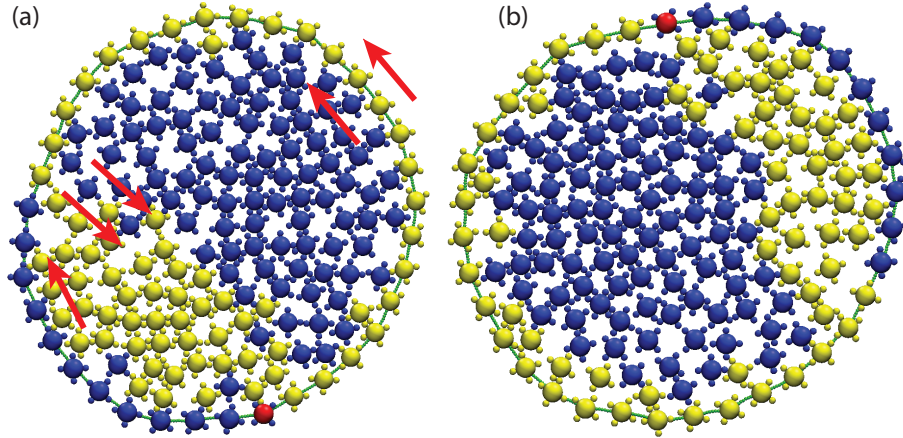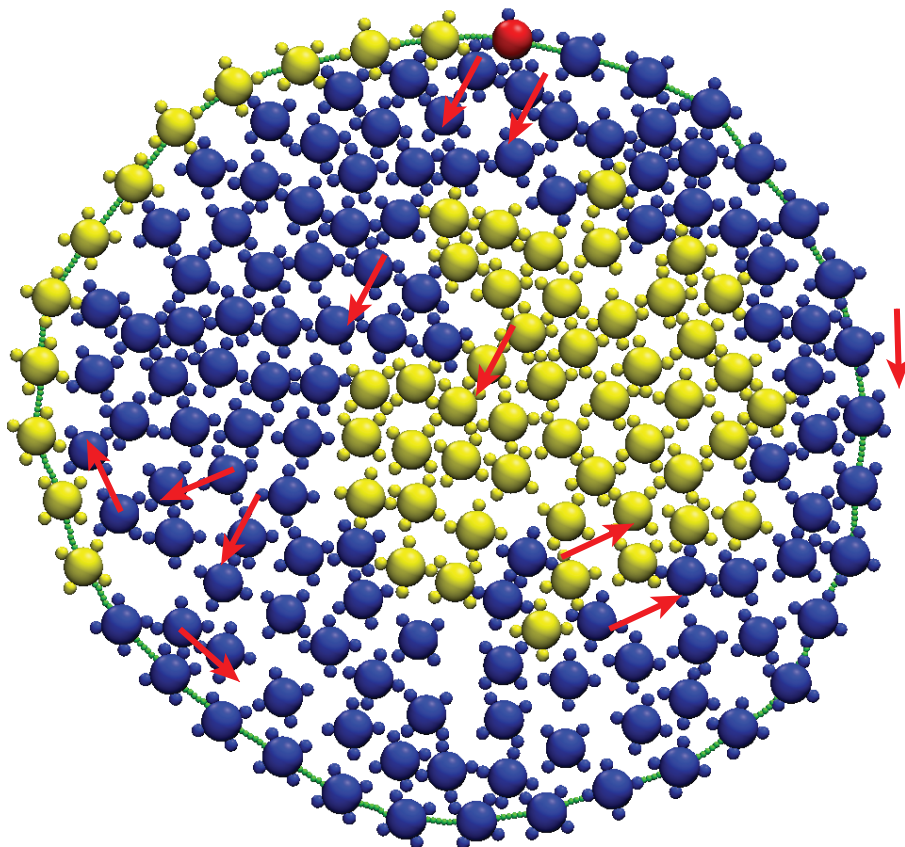
Figure 6.11 The interior spinners are driven oppositely by CW:CCW ratio of 67:33 while boundary spinners are driven oppositely by CW:CCW ratio of 33:67. (a) A snapshot of the system after 10000 time units. The interior spinners separate into a dynamic, imbalanced Janus-like particle. Each domain of like particles is in contact with the oppositely-driven boundary. The spinners' translational motion is illustrated by the red arrows. (b) Yellow spinners occasionally diffuse into the blue domain and translate along the boundary.

boundary is much stronger in this case as compared to the case where both the boundary and the interior have 50:50 ratio. It seems that the system fluctuates between two competing steady states: the Janus and the annulus (Fig. 6.8). We learned that when the boundary spinners are driven in only one direction, the system tends to form annuli of like particles. In this case, the majority spinner of the boundary (yellow) tends to drive the system to form an annulus configuration; however, having not enough like-rotating (yellow) spinners in the interior to spread along the boundary prevents it from doing so. In the following case, we will see when the majority spinners of the boundary and interior are of the same type, annulus configurations are favored.

Boundary and interior spinners each with 67:33 ratio of active spinners

In this case, the spinners of both the boundary and interior have a 67:33 ratio. The system forms an annulus of blue spinners (majority type) with yellow ones contained in the core (Fig. 6.12). The boundary rotates in clock-wise direction, the driving direction of a blue spinner. This configuration is structurally similar to that in Fig. 6.8 but is dynamically

Figure 6.12 A snapshot of the system after 10000 time units. The boundary and interior spinners are driven by 67:37 ratio. Instead of phase-separating into a Janus-like particle as one might expect, the interior spinners phase-separate into a moving core surrounded by oppositely particles that form complex vortices. The core seems to keep the same position relative to its boundary while the boundary is rotating clockwise. The spinners' translational motion is illustrated by the red arrows.

much more complex. Instead of moving in one direction as in Fig. 6.8, the blue spinners (majority type) move in two vortices that are separated by the two different portions of the boundary. The bigger vortex contains the core of yellow particles, which is rotating in the same direction of the vortex.

6.5 Discussion

Although the results in this Chapter are preliminary, they help qualitatively confirm the phenomena reported in Chapter 5 by the experiments. The results also suggest remarkable richness in the behavior of systems with flexible boundaries and open up further exciting
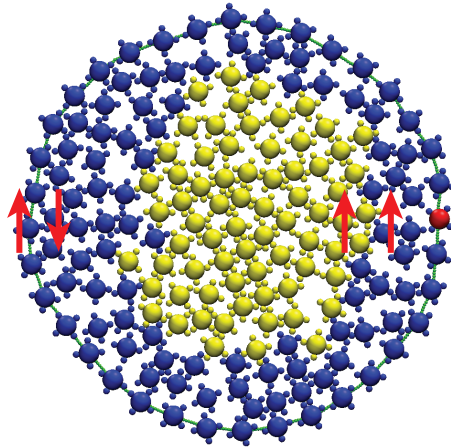
(a) The boundary spinners are driven in a single direction and the interior spinners are driven oppositely with CW:CCW ratio of 50:50.
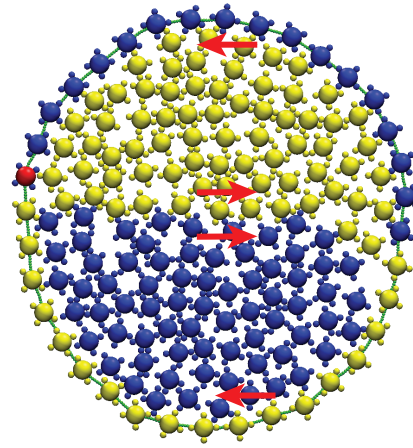
(b) The boundary and interior spinners each are driven oppositely with CW:CCW ratio of 50:50.
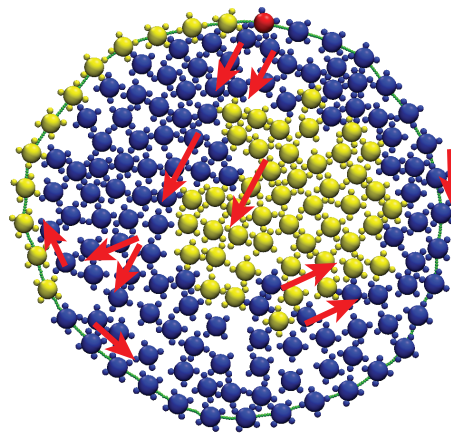
(c) The boundary and interior spinners each are driven oppositely with CW:CCW ratio of 67:33.
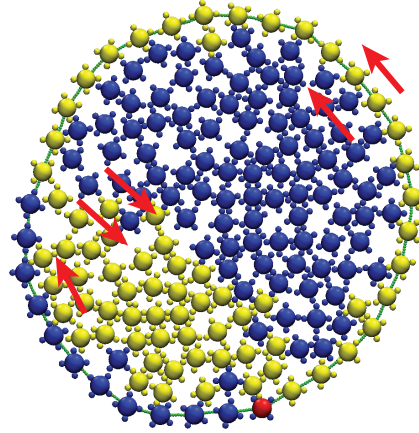
(d) The boundary and interiors spinners are driven oppositely with CW:CCW ratios of 33:67 and 67:33, respectively.

Figure 6.13 Summary of all studied cases with flexible boundaries. A driving torque of $\omega_0 = 1$ was used for all cases.

research. Quantifying the dynamics of the systems should be the immediate next steps and is likely to reveal how the boundaries influence the collective behavior of the interior particles. Quantities such as mean square displacement, kinetic and potential energy distributions, and "sticking" time between a pair of particles at different positions, are some important parameters to be investigated.

Beside exploring the current cases more deeply, other scenarios could be interesting to consider. One example is a system of driven boundary with non-driven or partially-driven interior spinners. The relevant questions are how a driven boundary influences the interior and is there a minimal composition of driven particles required to achieve curtain behavior? Secondly, using different patches of driven/non-driven spinners for a boundary one could potentially impart different kinds of dynamics in the interior. For example, can a dynamical quaternary Janus particle [158] be formed, instead of the binary version seen in the existing cases, by using a boundary of four alternatively driven patches? Lastly, varying parameters such as driving torque homogeneity and spring stiffness may impart interesting system behavior as well.

Beyond understanding the behavior of a system, one could imagine employ each of this flexibly confined system as molecular machines that can self-assemble or exhibit some interesting collective behavior. For an example, how a system of many rotating, flexible cells like that in Fig. 6.8 behave could be interesting: will they exhibit any effective interaction when the system is dense enough as individual driven spinners exhibit in bulk systems (Chapter 5)? What if different halves of the cells are rotating oppositely? One could also potentially utilize the collective rotation in imparting directional translation by setting up racks that the rotating cells can integrate and run on. A mixture of the dynamical Janus particles could exhibit interesting phenomena because they are much like normal Janus particles but, in addition, can interact dynamically with neighbors through their rotating spinners and boundaries.

Chapter 7

Conclusions and Outlook

7.1 Conclusions

Understanding how systems behave in regimes far from equilibrum is considered to be a key to realizing tomorrow's generation of smart materials that can adaptively and controllably change their properties on command. The knowledge can also be beneficial to a host of other fields, including distributed control of unmanned vehicles, assembly of mobile sensor networks, and transport, where engineering useful collective behavior out of individual agents or particles is important. Computer simulations hold a key to advancing the body of knowledge and high-performance computing is of particular importance. A vast parameter space and a lack of a governing theory all make high-speed computer simulations a necessary first step in a unified effort of tackling the challenge.

In this thesis, by utilizing high-performance codes, we make contributions to the field on three fronts. First, swarming behavior of interacting self-propelled particles in 3D (Chapter 4) has been investigated, yielding several new findings. A wide range of 3D swarming structures, many of which are reported for the first time, were discovered and characterized as a function of their interactions. The understanding of how the interaction potential influences system dynamics and morphology could potentially be helpful in engineering swarming systems with long-range interactions. We also reported novel properties of a system of SPP that includes sensitivity to initial conditions, swarm co-existence and different mechanisms of structural switching. Second, we reported the first systematic study of SRPs

(Chapter 5) that not only proposes a new alternative mechanism for driving a system out of equilibrum but also presents a remarkable wealth of dynamical and structural behavior. We found that a mixture of SRPs that are driven oppositely with a ratio 50:50 of CW:CCW exhibits spinodal decompositions in a manner similar to the equilibrium equivalent. In addition, we observed rotating crystals, cooperative and heterogeneous dynamics leading to super-diffusive motion, and complex phase behavior. This rich behavior of a simple model not only suggests even more exciting opportunities to investigate more complex systems but also presents an alternative route in understanding far-from-equilibirum behavior. Lastly, our preliminary work in confined systems (Chapter 6) of active particles demonstrates promising results and many interesting possibilities for engineering novel applications such as molecular machines. In addition, the confined systems are both simple and elegant enough to serve as experimental test beds for developing theory of far-from-equilibirum self-assembly.

7.2 Outlook

As the field is moving fast and gaining attention rapidly, there are many opportunities to explore. Below is a list of research directions that, we believe, are both exciting and immediately significant to advancing the current state of the art.

7.2.1 Self-assembly of driven shapes

The gear shape studied in Chapter 5 is a good example of how shape, when combined with activity, can give rise to rich behavior. Although we believe that the shape is not inherently responsible for the spinodal decomposition but rather it serves as a mechanism for energy transfer through collisions, shapes can greatly influence the system dynamics and morphology. For example, the square-lattice structure of the rotating crystals is a result of the gear shape. Imagine replacing the gear shape by other shapes such as triangles,

squares, hexagons or a mixture of different shapes: what sort of structures will the system adopt? How do shapes influence the nature of phase-separation and crystals growth? Is the cooperative and heterogeneous dynamics reported in Chapter 5 unique to geared shape? Similar questions may be asked regarding the role of shapes in self-propulsion.

7.2.2   Confined systems of active particles

Beyond the future work outlined in Chapter 6.5, confined systems of SPPs or of mixtures of SPPs and SRPs may be interesting. Studies of systems of self-propelled hard rods and bacteria confined in hard boundaries reported a tendency to aggregate to walls [65] and concentration-dependent collective behavior [153, 154, 155]. This suggests that confined systems of SPPs with flexible boundaries has the potential to be even richer in behavior. SPPs in a mixture with SRPs could impart motility to the (rotating or non-rotating) flexible cells (discussed in Chapter 5) and therefore make them behave in many ways similar to biological cells such as amoeba. Studies of such artificial "amoeba" could be very interesting and have far-reaching practical implications.

7.2.3   Active modifiers

How do a number of active particles change the behavior of an otherwise well-understood equilibrium system? An early study [159] has shown that doping a mixture of hard spheres with a small amount of active particles assists the coalescence of crystalline clusters and speeds up the crystallization dynamics at high densities. Systems of self-propelled hard spheres also exhibit a glass transition at a higher densities [160] and significantly shifted freezing densities [110] compared to equilibrium freezing of passive particles. Of course, not only the nature of the phase transitions could be influenced, but the dynamical and structural properties of the phases could potentially be modified by activity and shapes of the added particles. Examples of future studies in this direction include 1) a mixture

of passive shaped particles and smaller SPPs acting active "depletant" and 2) a confined system of passive shapes with a small number of SPRs. Potential outcomes include faster self-assembly, self-assembly with better yield, novel structures and new collective dynamics compared to the non-active equivalents.

7.2.4   3D systems

All the aforementioned directions of research could be done for both 2D and 3D. Most of the studies so far in active matter have been conducted in 2D. In 3D, however, a system may behave differently, especially for SRPs because going from 2D to 3D gives them two more rotation axes. Therefore, it will be harder for 3D versions of the SRPs in Chapter 5 to synchronize their rotational axes compared to in 2D. But it would be interesting if 3D SRPs align their rotational axes to form what we call a nematic spinner phase in which the spinners' rotations are synchronized. Furthermore, since most practical applications are in 3D, investigating 3D systems would potentially have wider-ranging implications.

Appendices

Appendix A

Supplementary materials for Chapter 4

A.1   Codes

The code for performing LD can be found in open-source package HOOMD Blue. Codes for simulating self-propelled particles and implementing the Morse potential can be found at codeblue.umich.edu repository, under SPPForce and SPPPotential plug-ins. A typical Python script for running a system of self-propelled particles is as following.

```
from hoomd_script import *
from hoomd_plugins import SPPPotential
from hoomd_plugins import SPPForce

import os
import random

#Packing fraction 0.03925 corresponds to 600 1-diameter partilces \
 in 20x20x20 box
system = init.read_xml(filename="data_hoomd_3DN600ri.xml")
random.seed(12345)
T=1.0
for p in system.particles:
```

```
        mass = p.mass;

        vx = random.gauss(0,T/mass)

        vy = random.gauss(0,T/mass)

        vz = random.gauss(0,T/mass)

        p.velocity = (vx,vy,vz)


# Intial run to randomize the particles
#assign WCA potential for the initial runs
slj = pair.slj(r_cut=2**(1.0/6.0))
slj.pair_coeff.set('A','A',epsilon=1.0,sigma=1.0)


#integrate.mode_standard(dt=0.005)
bd=integrate.bdnvt(group.all(), T=1.0, seed=12345)
bd.set_params(T=1.0)


#randomize the particles
run(1e5)


#disable lj interaction
lj.disable()


# Set noise level for the system
bd.set_params(T=0)


#apply morse potential
morse = SPPPotential.pair.morse_soft_core(r_cut=5.0)
morse.pair_coeff.set('A', 'A', Cr=0.5, lr=0.5, Ca=1.0, la=1.0)
```

```
# assign self-propelled force
sppforce = SPPForce.force.sppforce()
sppforce.set_coeff(1,0.5)

# dumping outputs
mol2=dump.mol2(filename="particle",period=1e5)
dump.dcd(filename="particle.dcd",period=1e4)
xml2=dump.xml(filename="particle",period=1e5)
xml2.set_params(velocity=True, acceleration=True)

analyze.log(quantities=['potential_energy',
              'kinetic_energy','temperature'], period=1000, \
                 filename='full.log')

dump.bin(file1="restart.1.bin.gz", file2="restart.2.bin.gz", \
   period=1e5)

run(1e6)
```

A.2 Videos

The videos of the swarms can be found on the Supplemental Materials of the paper [21], hosted by aps.org website `http://pre.aps.org/supplemental/PRE/v86/i1/e011136`.

Appendix B

Supplementary materials for Chapter 5

B.1 Codes

The code for performing LD can be found in open-source package HOOMD Blue. Codes for BD and simulating self-rotated particles can be found at codeblue.umich.edu repository, under BDIntegrator and SPPTorque plug-in. A typical Python script for running a system of self-rotated particles is listed below, followed by the code for calculating the structure factor in Chapter 5.

```python
# hoomd stuff
from hoomd_script import *
from math import sqrt
from hoomd_plugins.SPPTorque import spp_torque

# numeric stuff
import numpy as np
import math as m
import scipy.stats as sp
import random

# other stuff
```

```python
import os, sys

# intialize system
sys=init.read_xml("gear16384_phi04.xml")


# Assigning potential


#hardcore by WCA
slj = pair.slj(r_cut=2**(1.0/6.0))


# Standard slj for all particle types
slj.pair_coeff.set(sys.particles.types, sys.particles.types,\
epsilon=1.0, sigma=1.0)
slj.set_params(mode="shift")
nlist.reset_exclusions(['body', 'bond'])


# Creating groups
rigid=group.rigid()


#Dump outputs


#set dump xml
xml = dump.xml(filename="dump", period=1e5)
xml.set_params(position=True, velocity=True)


#set dump bin
```

```
dump.bin(file1="restart.1.bin.gz", file2="restart.2.bin.gz",\
  period=5e6)


#set log of thermodynamic quantities
logger1=analyze.log(quantities=['potential_energy',\
'kinetic_energy','temperature'],period=1e5, filename='full.log')


# Intergrator
integrate.mode_standard(dt=0.001)
bdnvt=integrate.bdnvt_rigid(group.all(),T=1,seed=12345)
#Set gamma
bdnvt.set_gamma('A', gamma=1, gammar=100)
bdnvt.set_gamma('B', gamma=1, gammar=100)


# enforce 2D simulation
update.enforce2d()


####Simulation parameters
#Driving torque
torque=100


#BD temperature or thermal noise
noise=0


#time to shrink box
#shrink_steps=1e5
```

```
#time to run at a constant density
t_steady=21e6


#fraction of bodies rotating CW
CWfrac=.5


#########Simulation runs


# adding self-rotated torques
spptorque = spp_torque.spptorque(group=rigid)
spptorque.set_coeff(0,0,torque,1,CWfrac)


#Set noise
bdnvt.set_params(T=noise)


# log msd for all rigid bodies
msd1 = analyze.msd(filename='msd_all.log', groups=[rigid],\
 period=1e3)


# create group of bodies rotating CW
tag_max = int(CWfrac*16384)
CW = group.tag_list(name="B", tags = range(0,tag_max))
CCW = group.tag_list(name="B", tags = range(tag_max, \
 16384))
# log msd for bodies rotating CW
msd2 = analyze.msd(filename='msd_CW.log', groups=[CW],\
 period=1e4)
```

```
msd3 = analyze.msd(filename='msd_CCW.log', groups=\
[CCW], period=1e4)
#set dump mol2
mol2 = dump.mol2(filename="dump", period=5e6)


#set dump dcd
dcd = dump.dcd(filename="dump.dcd", period=1e5)


#run 1mil steps at intial box size


run(t_steady)
```

The code for calculating the structure factor in Chapter 5 is listed below.

```
#include <iostream>
#include <fstream>
#include <vector>
#include <string.h>
#include<math.h>
#include <stdlib.h>
//#include "fftw3.h"
#include <stdio.h>
#include <gsl/gsl_math.h>
#include <gsl/gsl_sf_bessel.h>


#define PI   3.1415926
#define anint(x) ((x >= 0.5) ? (1.0) : (x < −0.5) ? (−1.0) : (0.0))
#define sign(x) ((x >0) ? (1.0) : (x < 0) ? (−1.0) : (0.0))
```

111

```cpp
using namespace std;

struct Particle
{
  int particleID;
  int visited;
  double vx, vy, vz;
  double x, y, z;
  double ax, ay, az;
  int cell; // cell index that the body containing the particle
  //belongs to
  int partype;
};

class system_of_par
  {
  public:
    vector <Particle> particle;
    double xcm, ycm, zcm;
    double vcmx, vcmy, vcmz;
    double acmx, acmy, acmz;
    double lx, ly, lz;
  };

void read_hoomd(char* filename, system_of_par& sys)
```

```cpp
{
  //this function read hoomd xml output file, and output
  //a system of particle
  int numparticle, parID =0, posmark1, posmark2,\
  numberlength1, numberlength2, l1, l2;
  double vx, vy, vz, x, y, z, ax, ay, az, lbox;
  char s1[100], s2[100], type[10], tempstr1[10], tempstr2[10];
  char* num;
  string buffer1, buffer2;
  size_t length1, length2;

  ifstream inFile(filename);

  // Extract the box dimension from the xml file in line
  //number 4

  // Just to skip 4 lines in the file − refer to an xml file
  for (int i=0; i<4; i++)
     inFile.getline(s1,100);

  buffer1 = s1;

  l1=buffer1.length();

  for (int j=1; j<=l1; j++)
  {
     if (buffer1.compare(j,2,"lx")==0)
```

113

```
  {
    posmark1=j+4;
  }


  if  (( buffer1 . compare ( j ,1 ,"\"")==0)&&( j <=15))
  {
    posmark2=j ;
  }


}


numberlength1=posmark2−posmark1 ;
length1 =buffer1 . copy ( tempstr1 , numberlength1 , posmark1 );
tempstr1 [ length1 ]= '\0 ';


lbox  =  atof ( tempstr1 );
sys . lx=lbox ;
sys . ly=lbox ;
sys . lz=lbox ;


// Extract  the  box  dimension  from  the  xml  file  in  line
// number  4


// Just  to  skip  1  more  line  in  the  file  to  the  line  number  5
// −refer  to  an  xml  file
for  ( int  i =0; i <1; i ++)
  inFile . getline ( s2 ,100);
```

```
buffer2 = s2;

l2=buffer2.length();

for (int j=1;j<=l2;j++)
{
  if (buffer2.compare(j,3,"num")==0)
  {
    posmark1=j+5;
  }

  if (buffer2.compare(j,1,"\"")==0)
  {
    posmark2=j;
  }

}

numberlength2=posmark2-posmark1;
length2=buffer2.copy(tempstr2,numberlength2,posmark1);
tempstr2[length2]='\0';

numparticle = atoi(tempstr2);

Particle p[numparticle];
```

```
// Read cordinates
for (int i=0;i<numparticle;i++)
{
  inFile >>x>>y>>z;
  p[i].particleID=parID;
  p[i].x=x;
  p[i].y=y;
  p[i].z=z;
  p[i].visited =0;
  parID+=1;
  p[i].partype=1;
}



// Skip a number of  lines to jump to the velocity portion in
// the xml file

//   for (int i=0;i<numparticle+5;i++)
for (int i=0;i<3;i++)
{
  inFile.getline(s1,100);
}


// Read velocity
for (int i=0;i<numparticle;i++)
{
  inFile >>vx>>vy>>vz;
```

```cpp
      p[i].vx=vx;
      p[i].vy=vy;
      p[i].vz=vz;
      sys.particle.push_back(p[i]);


    }


    /*   // Skip another 2 lines to jump to the acceleration
    // portion in the xml file

     for (int i=0;i<3;i++)
     {
     inFile.getline(s,100);
     }
     */



}

void center_of_mass(system_of_par& sys)
{
  // this function finds the center of mass of a system.
  sys.xcm=0;
  sys.ycm=0;
  sys.zcm=0;
  sys.vcmx=0;
  sys.vcmy=0;
```

```
sys.vcmz=0;
sys.acmx=0;
sys.acmy=0;
sys.acmz=0;


int i, numofpar;
numofpar=sys.particle.size();


for (i=0; i<numofpar; i++)
{
  sys.xcm += sys.particle[i].x;
  sys.ycm += sys.particle[i].y;
  sys.zcm += sys.particle[i].z;
  sys.vcmx += sys.particle[i].vx;
  sys.vcmy += sys.particle[i].vy;
  sys.vcmz += sys.particle[i].vz;
  sys.acmx += sys.particle[i].ax;
  sys.acmy += sys.particle[i].ay;
  sys.acmz += sys.particle[i].az;
}

sys.xcm /= numofpar;
sys.ycm /= numofpar;
sys.zcm /= numofpar;
sys.vcmx /= numofpar;
sys.vcmy /= numofpar;
sys.vcmz /= numofpar;
```

```
sys.acmx /= numofpar;
sys.acmy /= numofpar;
sys.acmz /= numofpar;




}




double distance (Particle p1, Particle p2, double Lx, double
\Ly, double Lz)
{

  // Calculate distance between two particles in box by \
  //Lx-Ly-Lz
  double dx, dy, dz, r;

  dx = p1.x - p2.x;
  dy = p1.y - p2.y;
  dz = p1.z - p2.z;

  // Counter potential pbc effects

  dx -= Lx * anint(dx / Lx);
  dy -= Ly * anint(dy / Ly);
  dz -= Lz * anint(dz / Lz);
  r = sqrt(dx * dx + dy * dy + dz * dz);
```

```
    return r;



}



// function ifSameParType determines whether two bodies
// are same type
// Bodies with idices greater than a threshold than they rotating
//CCW, otherwise CW
bool ifSameParType ( int i, int j, int separator)
{
   if ( (i> separator) && (j > separator))
   {
     return true;
   }
   else if ( (i<= separator) && (j <= separator))
       return true;
   else
   {
     return    false;
   }


}



unsigned int factorial(unsigned int n)
{
    if (n == 0)
    return 1;
```

```
    return n * factorial(n - 1);
}


// real coordinate distance between two particles are smaller
// or equal than half of the box size
// from all 3 dimension
// If the coordinate distance between two particles
// is greater than half of the box size
// then the distance needs to be accounted for periodic
// boundary condition
void boxWrapper(double& dx, double& dy, double& dz, \
double Lx, double Ly, double Lz)
{
  // dx, dy, dz are coordinate distance and Lx, Ly, Lz
  // are box lengths
  if ((dx>=Lx/2) || (dx<=-Lx/2))
    dx = dx - sign(dx)*Lx;


  if ((dy>=Ly/2) || (dy<=-Ly/2))
    dy = dy - sign(dy)*Ly;


  if ((dz>=Lz/2) || (dz<=-Lz/2))
    dz = dz - sign(dz)*Lz;
}


// Structure factor: classical way - reference to
// "Computer simulation of liquids"
```

```cpp
void structure_factor_1d(double* r, double* g, int nBinRdf,\
int nBinStruc, double bulkDensity, double* k, double* S, \
double L)
{

  int i, j;
  double dr = r[1] - r[0];
  double kr, Jo;

  // ofstream ofs;
  // double fs = 1.0 / (r[1] - r[0]);
  // double fspan = fs / 2.0;
  // double dq = fspan / nBins;
  // S[0]=0;
    for (i=0; i<nBinStruc; i++)
  {

    k[i] = 2*PI*i/L;



    for (j=0; j<nBinRdf; j++)
    {
      kr = k[i] * r[j];
      // estimate zero Bessel function of first kind
       Jo = gsl_sf_bessel_J0(kr);
        S[i] += (g[j]-1) * Jo * r[j]* dr;
    }
```

```
      S[i] = 1+2*PI* bulkDensity* S[i];
  }
}


// direct calculation: looping over all pairs of particles

void structure_factor(Particle* bodyArray, int numBody, int \
nBinStruc, double* kx, double* ky, double **S2, double L)
{
  double coskr, sinkr;

  // Initialize wave vector
  for (int i=0; i<nBinStruc; i++)
  {
    kx[i] = 2*PI*i/L;
    ky[i] = 2*PI*i/L;
  }

  for (int i=0; i<nBinStruc; i++)
    for (int j=0; j<nBinStruc; j++)
    {

      coskr=0;
      sinkr=0;
      for (int n=0; n<numBody; n++)
      {
        coskr += cos(kx[i]*bodyArray[n].x +\
```

```
            ky[j]*bodyArray[n].y);

        sinkr += sin(kx[i]*bodyArray[n].x +\
        ky[j]*bodyArray[n].y);

        }


        S2[i][j] = (coskr*coskr + sinkr*sinkr)\
        /numBody;

        }


}


/*
 void structure_factor(double* r, double* g, int nBins,\
  double bulkDensity)
 {
 int i, nc;
 fftw_complex *out;
 fftw_plan plan_forward;


 nc = (nBins / 2) + 1;


 out = (fftw_complex*)fftw_malloc(sizeof(fftw_complex) * nc);


 plan_forward = fftw_plan_dft_r2c_1d(nBins, g, out, \
 FFTW_ESTIMATE);


 fftw_execute(plan_forward);
```

```cpp
  ofstream ofs;

  double fs = 1.0 / (r[1] - r[0]);

  double fspan = fs / 2.0;


  ofs.open("S_q.txt");

  ofs << "q\tS\n";

  for (i=0; i<nc; i++)

  {

  double q = i * fspan / nc;

  out[i][0] /= nc;

  out[i][1] /= nc;

  ofs << q << "\t" << sqrt(out[i][0] * out[i][0] + out[i][1] *\

   out[i][1]) << std::endl;

  }


  ofs.close();



  fftw_destroy_plan(plan_forward);

  fftw_free(out);

  }

*/


/* // Filon's sine transformation

  void structure_factor_1d(double* r, double* g, int nBins, \

  double bulkDensity, double* q, double* S)
```

```cpp
{
cout << "Ref: Filon's sine transformation\n";

int i, j;
double dr = r[1] - r[0];

ofstream ofs;
double fs = 1.0 / (r[1] - r[0]);
double fspan = fs / 2.0;
double dq = fspan / nBins;


double theta, sintheta, costheta, sintheta2, costheta2,\
theta2, theta3;
double fourPI, alpha, beta, gamma, Se, So;
fourPI = 16.0 * atan(1.0);

for (i=0; i<nBins; i++)
{
q[i] = (i + 0.5) * dq;
theta = q[i] * dr;
sintheta = sin(theta);
costheta = cos(theta);
sintheta2 = sintheta * sintheta;
costheta2 = costheta * costheta;
theta2 = theta * theta;
theta3 = theta * theta2;
```

```
if (theta < 1e-6)
{
alpha   = 0.0;
beta    = 2.0 / 3.0;
gamma   = 4.0 / 3.0;
}
else
{
alpha   = (1.0/theta3) * (theta2 + theta * sintheta *\
 costheta - 2.0 * sintheta2);
beta    = (2.0/theta3) * (theta * (1.0 + costheta2) - \
2.0 * sintheta * costheta);
gamma   = (4.0/theta3) * (sintheta - theta * costheta);
}


// The integral is g(r) * r for the 3D transform


// Do the sum over the even ordinates
Se = 0.0;
for (j=0; j<nBins; j+=2)
Se += (g[j] - 1) * r[j] * sin(q[i] * r[j]);


// Subtract half the first and last terms: here g[0] = 0.0
Se -= 0.5 * ((g[nBins-1] - 1) * r[nBins-1] * sin(q[i] *\
 r[nBins-1]));
```

```cpp
// Do the sum over the odd ordinates
So = 0.0;
for (j=1; j<=nBins-1; j+=2)
So += (g[j] - 1) * r[j] * sin(q[i] * r[j]);



S[i] = (-alpha * (g[nBins-1] - 1) * r[nBins-1] * \
cos(q[i] * r[nBins-1]) + beta * Se + gamma * So) * dr;



// Include normalizing factor
S[i] = 1 + fourPI * bulkDensity * S[i] / q[i];


}
}
*/



/*
// Structure factor: Escobedo's method
void structure_factor_1d(vector<_vertex>& \
vertices,
double Lx, double Ly, double Lz, \
vector<double>& q, vector<double>& S)
{
  cout << "Ref: Escobedo's method\n";
```

```cpp
int i, nNumBeads, x, y, z, nBins=5;
ofstream ofs;


vector<double> S, q;
double magq, magS, term1, term2, qdotr;
double twoPI = 8.0 * atan(1.0);


nNumBeads = vertices.size();
   for (x=0; x<nBins; x++)
   for (y=0; y<nBins; y++)
     for (z=0; z<nBins; z++)
     {
       if (x==0 && y==0 && z==0)
         continue;


       magq = twoPI * sqrt(x * x \
       / (Lx * Lx)\
        + y * y / (Ly * Ly) + z * z]\
         / (Lz * Lz));
       q.push_back(magq);


       term1 = 0.0;
       term2 = 0.0;
       for (i=0; i<nNumBeads; \
       i++)
       {
```

```cpp
                    qdotr = twoPI * (x / \
                    Lx * vertices[i].x\
                     + y / Ly * vertices[i].y\
                      + z / Lz * vertices[i].z);
                   term1 += sin(qdotr);
                   term2 += cos(qdotr);
              }


              magS = (term1 * term1 +\
               term2 * term2)\
               / nNumBeads;
              S.push_back(magS);
         }

   ofs.open("S_q.txt");
   ofs << "q\tS\n";
   for (i=0; i<q.size(); i++)
   {
     ofs << q[i] << "\t" << S[i] << std::endl;
   }

   ofs.close();


} */
```

```cpp
int main (int argc, char** argv)
{
    int nBinRdf, nBinStruc, ibin;
    double *r,*g,*x,*y,*z,*k,*kx,*ky,*S,vb,dist,\
    dr,dx,dy,dz,r2;

    system_of_par sysofpar;
    int numparticle, ParPerBody=5, numbody;
    double CWfrac;

    ofstream outFile1, outFile2;
    double Lx,Ly, Lz;

    // get the file name and other input parameters
    ifstream inFile(argv[1]);
    //get the bin number for the rdf
    nBinRdf = atoi(argv[2]);
    //get the bin number for the struc
    nBinStruc = atoi(argv[3]);
    //percentage of bodies rotating CW
    CWfrac = atof(argv[4]);

    r = new double [nBinRdf];
    g = new double [nBinRdf];
    k = new double [nBinStruc];
    kx = new double [nBinStruc];
    ky = new double [nBinStruc];
```

```
S = new double [ nBinStruc ];


// read the input file
 read_hoomd ( argv [1] , sysofpar );


// number of particle
numparticle=sysofpar . particle . size ();
numbody = numparticle / ParPerBody ;


int numbody_CW = int (numbody*CWfrac +0.5);
int numbody_CCW = numbody − numbody_CW ;



// box sizes
Lx=sysofpar . lx ;
Ly=sysofpar . ly ;
Lz=sysofpar . lz ;
// Initialize vector x,y,z
x= new double [ numparticle ];
y= new double [ numparticle ];
z= new double [ numparticle ];
dr = Lx /2.0/ nBinRdf ; // Lx=Ly
for ( int i =0;i<numparticle ; i++)
{
  x[ i ]=sysofpar . particle [ i ]. x ;
  y[ i ]=sysofpar . particle [ i ]. y ;
  z[ i ]=sysofpar . particle [ i ]. z ;
```

```
    }


    // creating vector of the center of masses
    Particle * bodyCOM = new Particle[numbody];


    int bodycount=0;


    for (int i=0; i<numparticle; i++)
    {
      if ((i+1)%ParPerBody==0 )
      {
        bodyCOM[bodycount]=\
        sysofpar.particle[i];
        bodycount+=1;
      }


    }


// Calculate g(ibin)
    for (int i=0; i<nBinRdf; i++)
    {
      g[i] = 0.0;
      r[i]=0.0;
    }
    for (int i=0; i<nBinStruc; i++)
    {
      S[i] = 0.0;
```

```
    k[i] = i*2*PI/Lx;
    kx[i]=0.0;
    ky[i] =0.0;
}


int indexi, indexj; \
// indices of the central disks of the gears

for (int i=0;i<numbody-1;i++)
  {
    indexi = i*5+4;


    for (int j=i+1;j<numbody;j++)
      {
        indexj = j*5+4;
        dx=x[indexi]-x[indexj];
        dy=y[indexi]-y[indexj];
        dz=z[indexi]-z[indexj];


        boxWrapper(dx,dy,dz,Lx,\
        Ly,Lz);



        r2= dx*dx+dy*dy+dz*dz;
        dist = sqrt(r2);


        ibin=(int)(dist/dr);
```

134

```
            if (ibin<nBinRdf)

            {


              if ( ifSameParType\
            (indexi,indexj,\
             numbody_CW*5-1) )
                  g[ibin]+=2;
              //   else
                //   g[ibin]-=2;
            }

         }

     }


   double bulkDensity, factor, Nideal;
   bulkDensity= (double)numbody/(Lx*Ly);


// factor = 4.0 * PI * pow(dr, 3.0) / 3.0; //for 3D
   factor = PI * pow(dr, 2.0);   // 2d
   for (int i=0; i<nBinRdf; i++)
     {
       r[i] = (i + 0.5 + 1) * dr/10; \
       //dividing the radius by particle diameter


       //vb =  factor * (pow(i+1, 3.0) - \
       pow(i, 3.0)); //for 3D


       vb =  factor * (pow(i+1, 2.0) - \
```

135

```cpp
        pow(i, 2.0)); // 2d
        Nideal = vb * bulkDensity;


        g[i] = g[i]*2 / (numbody * Nideal);
    }


// Create output file for rdf
    outFile1.open("rdf_spin.txt");
        for (int i=0;i<nBinRdf;i++)
            outFile1<<r[i]<<"\t"<<g[i]<<endl;
    outFile1.close();


    // set first element of S
    //S[0]=0;


//   structure_factor_1d(r, g, nBinRdf,nBinStruc,\
  bulkDensity, k, S, Lx);


    double** S2 = new double*[nBinStruc];
    for (int n=0;n<nBinStruc;n++)
    {
        S2[n] = new double[nBinStruc];
    }


    structure_factor(bodyCOM, numbody_CW,\
    nBinStruc, kx,ky, S2, Lx);
```

```cpp
// calculate S from averaging S2 at fixed wave \
vector magnitute
int counter;
for (int n=0;n<nBinStruc;n++)
{
  counter = 0;
  for (int i=0;i<nBinStruc;i++)
    for (int j=0;j<nBinStruc;j++)
    {
      if ((n*n<=(i*i+j*j)) && \
      ((n+1)*(n+1) > (i*i+j*j)))
      {
        S[n] +=S2[i][j];
        counter +=1;
      }
    }
  if (counter >0)
  S[n] /= counter;
}

outFile2.open("strucFact.txt");
for (int i=1;i<nBinStruc;i++)
  outFile2<<k[i]<<"\t"<<S[i]<<endl;
outFile2.close();

inFile.close();
```

```
    delete [] g;

    delete [] r;

    delete [] k;

    delete [] kx;

    delete [] ky;

    delete [] S;

    delete [] x;

    delete [] y;

    delete [] z;

    delete [] bodyCOM;


    for (int i=0;i<nBinStruc;i++)

      delete [] S2[i];

    delete [] S2;


    return 0;


}
```

B.2   Movies and Figures

This Supplementary Materials section contains representative snapshots from each movie
and figures supplementing the discussion of the main text.

B.3   Non-equilibrium phase boundaries

The non-equilibrium phase boundaries are extracted from simulation data as follows:

- *Frozen state to fluid.* This transition is easily detected by a jump in the ratio of translational to total kinetic energy κ as a function of density, see Fig. 1(b). The transition is discontinuous and thus the boundary is indicated by a solid line in Fig. 1(c).
- *Phase separated fluid to rotating crystal.* This transition is quantified through the crystal fraction χ, see Fig. B.9. We typically observe coexistence between the phase separated fluid and the rotating crystal in our simulations and do not attempt to determine the coexistence region precisely. Instead, we only determine the density where crystallization is first observed in simulation. The transition is discontinuous and thus the boundary is indicated by a solid line in Fig. 1(c).
- *Mixed fluid to phase separated fluid.* This transition seems to be continuous, but is more complicated due to critical fluctuations, which will be explored elsewhere. For the current work we analyze the domain size growth as a function of time, see Fig. B.9, and search for appearance of its divergence. We indicate the boundary by a dashed line in Fig. 1(c).

As the applied torque is decreased in our simulations in the absence of noise (ω_0 as low as 0.01 in Fig. 1(c)), the dynamics slows down. Phase separation and the appearance of rotating crystals are not affected by the slowdown. If the torque is exactly zero, there is no dynamics in the system and we cannot study its time evolution. In practice, however, there is always some noise which will compete with the active torque: in the case where the active torque is low enough (or zero) that noise dominates over it, equilibrium behavior is recovered continuously.

B.4   Effective demixing potential

This section contains a derivation and discussion of the effective demixing potential for the interaction of two B spinners in a dense matrix of A spinners.

We start with the single particle density function for an individual particle i at position $\vec{r}_i$,

$$\rho_i(\vec{r}) = \delta(\vec{r} - \vec{r}_i). \tag{B.1}$$

It can be extended to the two spinner types,

$$\begin{aligned}
\rho_A(\vec{r}) &= \sum_{i \in A} \delta(\vec{r} - \vec{r}_i), \\
\rho_B(\vec{r}) &= \sum_{i \in B} \delta(\vec{r} - \vec{r}_i),
\end{aligned} \tag{B.2}$$

where $i \in A$ and $i \in B$ mean that particle i is of type A and B, respectively. We assume there are N_A particles of type A and N_B particles of type B moving in a system of volume V. The pair correlation function is defined as

$$\begin{aligned}
g_{IJ}(\vec{r}_1, \vec{r}_2) &= \frac{\langle \rho_I(\vec{r}_1)\rho_J(\vec{r}_2) \rangle}{\langle \rho_I \rangle \langle \rho_J \rangle} \\
&= \frac{V^2}{N_I N_J} \langle \rho_I(\vec{r}_1)\rho_J(\vec{r}_2) \rangle,
\end{aligned} \tag{B.3}$$

where $I, J \in \{A, B\}$. By taking into account translational symmetry, we can write

$$\begin{aligned}
g_{IJ}(\vec{r}) &:= g_{IJ}(\vec{0}, \vec{r}) = \frac{1}{V} \int_V g_{IJ}(\vec{r}', \vec{r}' + \vec{r}) \, d\vec{r}' \\
&= \frac{V}{N_I N_J} \int_V \langle \rho_I(\vec{r}')\rho_J(\vec{r}' + \vec{r}) \rangle \, d\vec{r}' \\
&= \frac{V}{N_I N_J} \sum_{i \in I} \sum_{j \neq i \in J} \langle \delta(\vec{r} - (\vec{r}_i - \vec{r}_j)) \rangle,
\end{aligned} \tag{B.4}$$

and since particles of the same type are identical,

$$\begin{aligned}
g_{AA}(\vec{r}) &= V \frac{N_A - 1}{N_A} \langle \delta(\vec{r} - (\vec{r}_{a_1} - \vec{r}_{a_2})) \rangle, \\
g_{BA}(\vec{r}) &= V \langle \delta(\vec{r} - (\vec{r}_a - \vec{r}_b)) \rangle, \\
g_{BB}(\vec{r}) &= V \frac{N_B - 1}{N_B} \langle \delta(\vec{r} - (\vec{r}_{b_1} - \vec{r}_{b_2})) \rangle,
\end{aligned} \tag{B.5}$$

where $a, a_1, a_2 \in A$ and $b, b_1, b_2 \in B$. Finally, we can calculate the radial distribution

functions (RDFs) from simulation (shown in Fig. B.7) using this equation:

$$g_{IJ}(r) = \lim_{\Delta r \to 0} \frac{1}{2\pi r \Delta r} \int_{r \leq \|\vec{r}\| \leq r + \Delta r} g_{IJ}(\vec{r}) \, d\vec{r}. \tag{B.6}$$

We now map the non-equilibrium system of rotationally driven spinners on an equilibrium system of isotropic particles interacting with pair potentials. The mapping is achieved by determining pair potentials $U_{AA}(r)$, $U_{AB}(r)$, $U_{BB}(r)$ that give rise to RDFs similar to the RDFs $g_{AA}(r)$, $g_{AB}(r)$, $g_{BB}(r)$ observed in simulation. Note that symmetry dictates the equality of the potentials for like-particle interactions: $U_{AA}(r) = U_{BB}(r)$.

In the limit of a strong majority of component A, the pair potential for the B particles can be estimated via the potential of mean force,

$$U_{BB}(r) = -kT \lim_{n_B \to 0} \log g_{BB}(r), \tag{B.7}$$

where $n_B = N_B/(N_A + N_B)$. Furthermore, we can approximate the potential for unlike-particle interactions using the same method:

$$U_{BA}(r) \approx -kT \lim_{n_B \to 0} \log g_{BA}(r). \tag{B.8}$$

This is indeed an approximation, because unlike in the situation for U_{BB} where each B particle is usually surrounded by only one other B particle, the B particle will have several A neighbors. This means $g_{BA}(r)$ includes many-particle effects and is not fully describable by a pair potential approximation.

The quantity responsible for inducing spinodal decomposition is the energy difference $U_{ED}(r) = U_{AA}(r) + U_{BB}(r) - 2U_{BA}(r)$. We call this difference the *effective demixing (ED) potential*. Using the approximations above we can write

$$U_{ED}(r) = -kT \lim_{n_B \to 0} \log \left(\frac{g_{BB}(r)}{g_{BA}(r)} \right). \tag{B.9}$$

A value $U_{\text{ED}}(r) < 0$ indicates a preference for demixing at distance r. If the particles A and B are indistinguishable, for example in a system of non-driven spinners, then the potential vanishes: $U_{\text{ED}}(r) = 0$.

The *effective demixing force* is the gradient of the effective demixing potential,

$$\vec{F}_{\text{ED}}(r) = -\nabla U_{\text{ED}}(r). \tag{B.10}$$

It is an indicator for how strongly like particles are being pushed together on the expense of unlike-particle contacts. In other words, it is a measure for the strength of spinodal decomposition. $\vec{F}_{\text{ED}}$ is an effective force that could be measured directly in experiment, for example using optical tweezers for colloids. We can therefore say that like particles are "sticky" or that they feel an "effective attraction" favoring the local aggregation of particles of the same type.
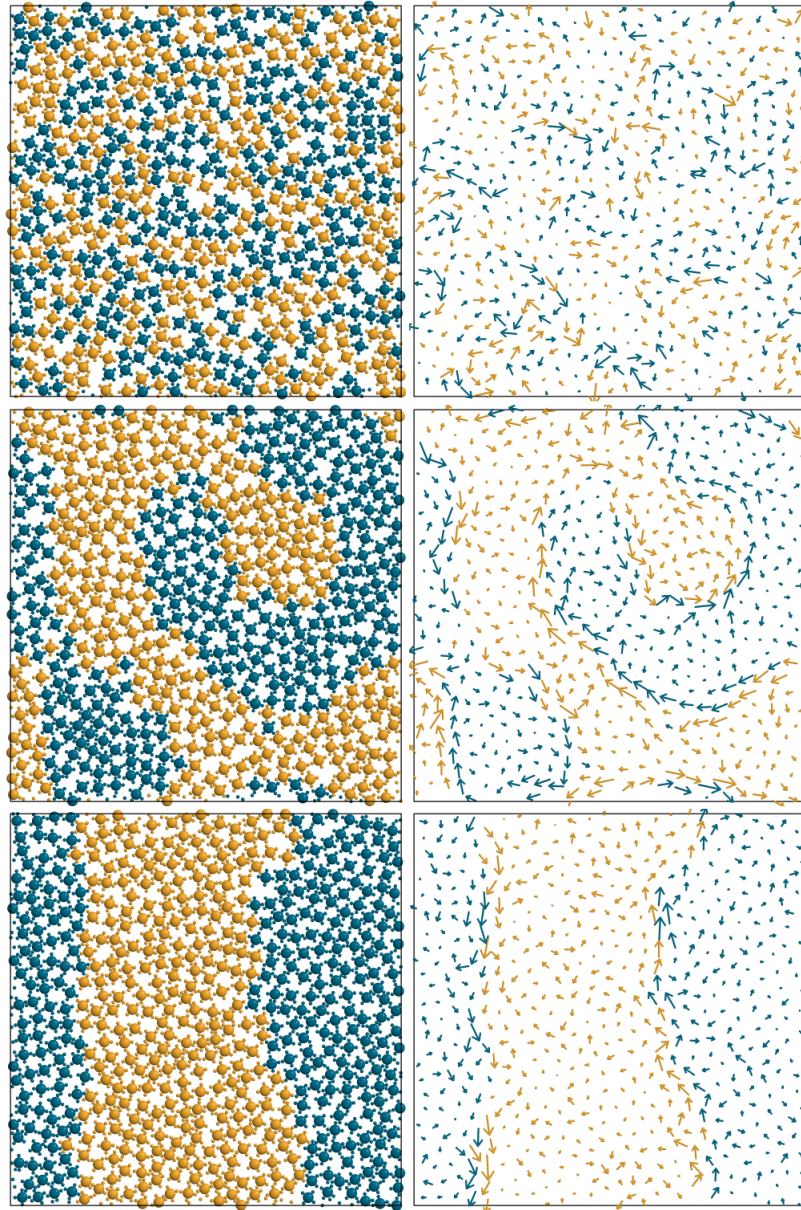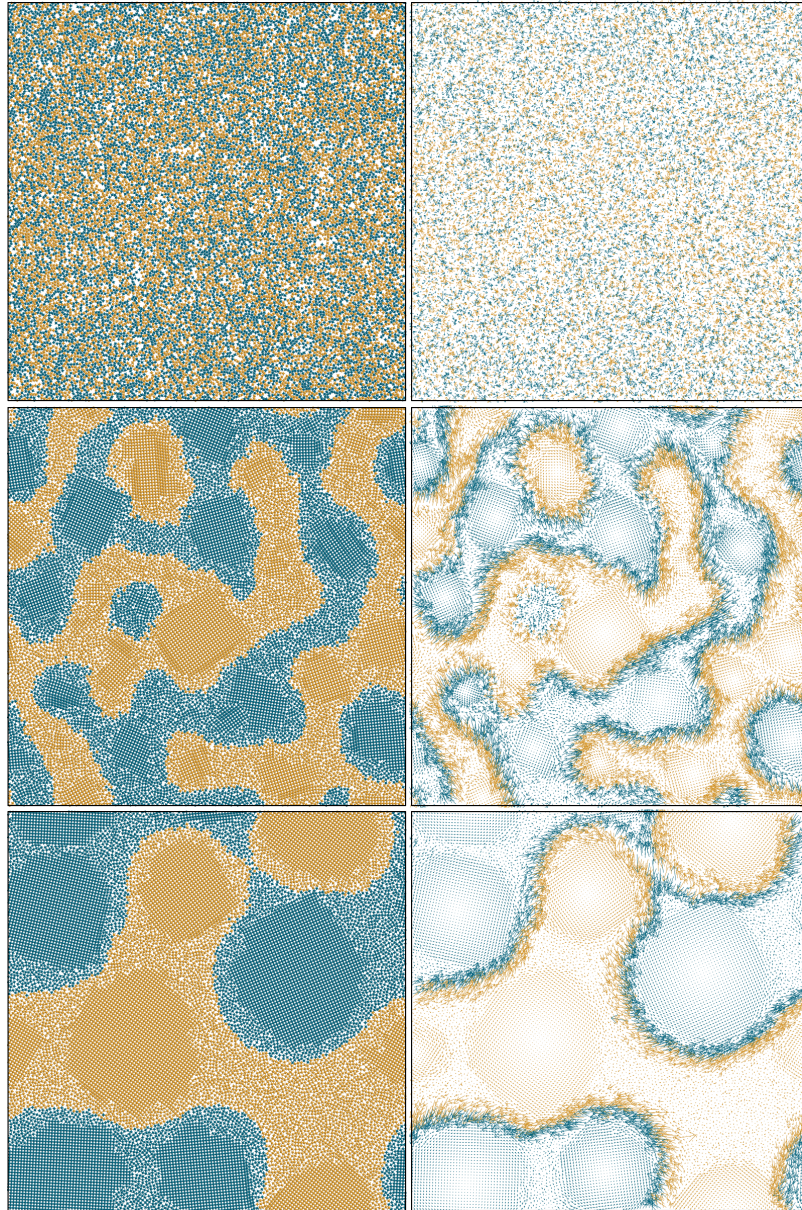
Figure B.1 *Snapshots from Movie 1.* A binary system of $N = 576$ spinners, where half of the spinners rotate clockwise and the other half rotate counter-clockwise. Simulation parameters: $\phi = 0.5$, $\omega_0 = 1$, $T^* = 0$. The movie shows spinners (left column) and vector plots of the short-time diffusion $\Delta x(10t_0)$ (right column) at three different times during spinodal decomposition. The simulation starts from an initially mixed configuration (top row, $t = 0$) and proceeds through phase separation (middle row, $t = 1,000t_0$), until in steady state two vertical stripes are formed (bottom row, $t = 5,000t_0$). From Ref. [23].
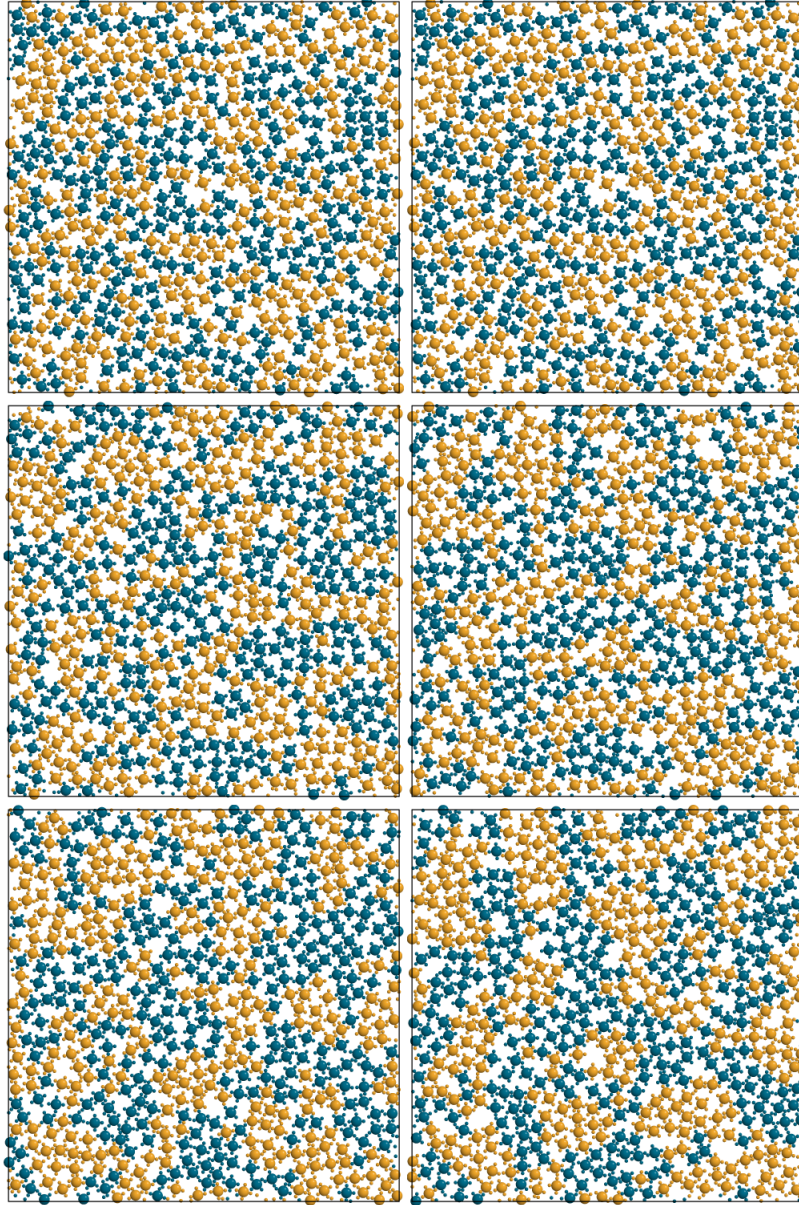
143
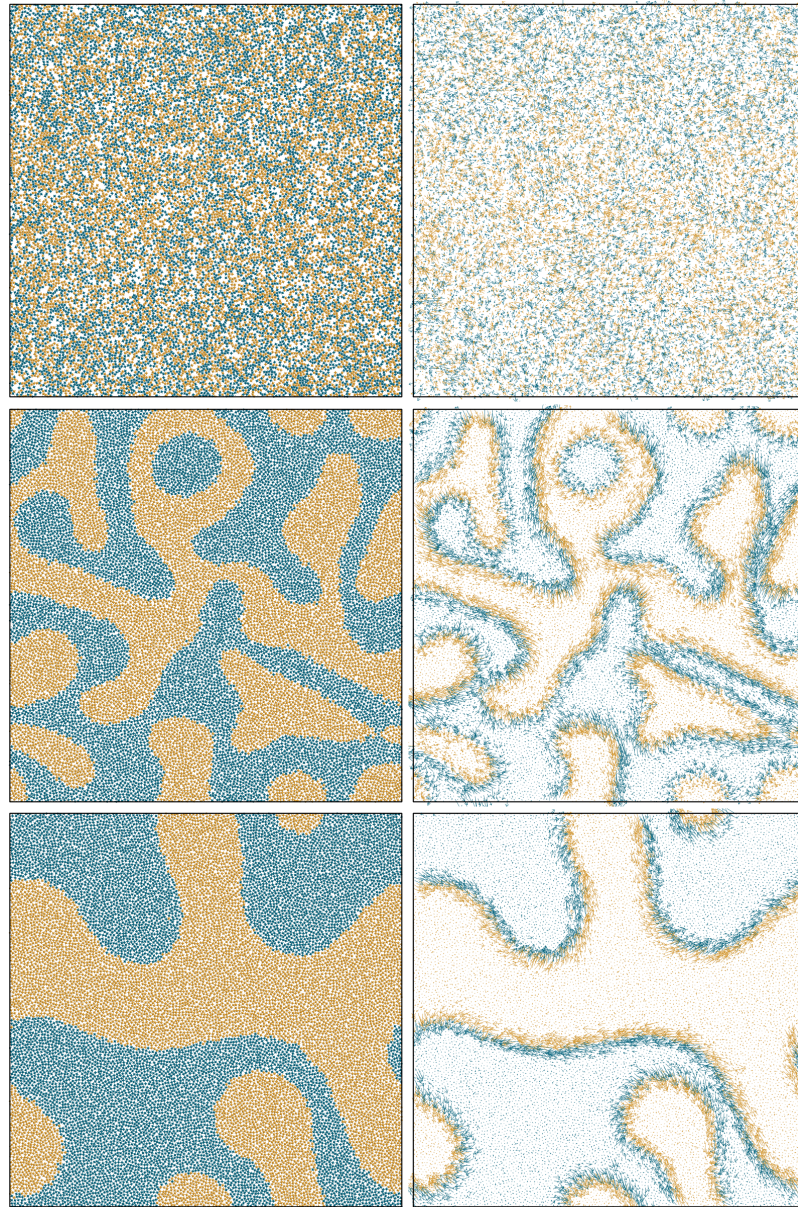
Figure B.2 *Snapshots from Movie 2.* A binary system of $N = 16{,}384$ spinners, where half of the spinners rotate clockwise and the other half rotate counter-clockwise. Simulation parameters: $\phi = 0.5$, $\omega_0 = 1$, $T^* = 0$. The movie shows spinners (left column) and vector plots of the short-time diffusion $\Delta x(100t_0)$ (right column) at three different times during spinodal decomposition. The simulation starts from an initially mixed configuration (top row, $t = 0$) and proceeds through phase separation (middle row, $t = 1{,}000t_0$). At the end of the simulation, steady state is not yet reached (bottom row, $t = 10{,}000t_0$). From Ref. [23].

Figure B.3 *Snapshots from Movie 3.* A binary system of $N = 16,384$ spinners, where half of the spinners rotate clockwise and the other half rotate counter-clockwise. Simulation parameters: $\phi = 0.6$, $\omega_0 = 1$, $T^* = 0$. The movie shows spinners (left column) and vector plots of the short-time diffusion $\Delta x(100t_0)$ (right column) at three different times during simultaneous spinodal decomposition and the formation of rotating crystal within single component domains. The simulation starts from an initially mixed configuration (top row, $t = 0$) and proceeds through phase separation (middle row, $t = 1,000t_0$). At the end of the simulation, steady state is not yet reached (bottom row, $t = 10,000t_0$). From Ref. [23].
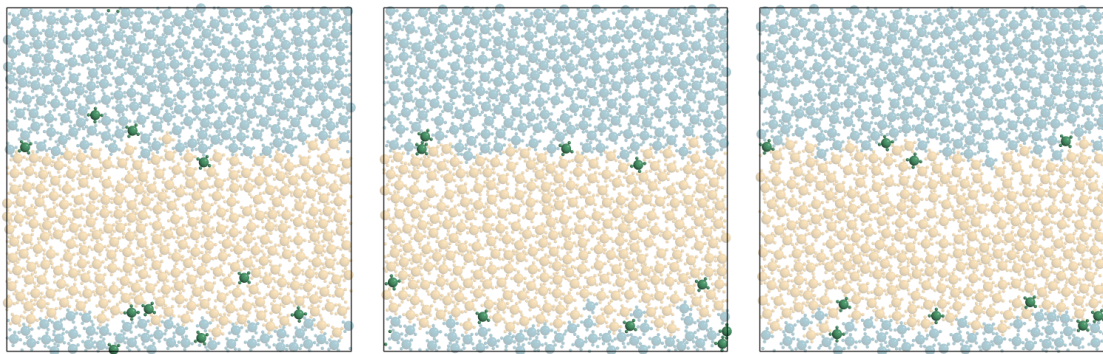
**Figure B.4** *Snapshots from Movie 4.* Ten inactive particles (dark green) immersed into phase separated system of an even mixture of $N = 566$ spinners (light blue and orange). Simulation parameters: $\phi = 0.5$, $\omega_0 = 1$, $T^* = 0$. The inactive particles are observed moving along the interface. Snapshots are shown through time: $t = 0$ (left), $t = 3,000t_0$ (middle), $t = 6,000t_0$ (right). From Ref. [23].

Figure B.5 *Snapshots from Movie 5.* Comparison of Langevin Dynamics (left side) and Brownian Dynamics (right side) in simulations with fine time resolution ($0.1t_0$ between two consecutive snapshots in the videos). Particles' positions fluctuate more in the Brownian Dynamics simulation (because of noise and the absence of inertia), but otherwise the systems behave very similarly with both simulation techniques. A binary system of $N = 576$ spinners, where half of the spinners rotate clockwise and the other half rotate counter-clockwise. Simulation parameters: $\phi = 0.5$, $\omega_0 = 1$, $T^* = 0$. The simulation starts from an initially mixed configuration (top row, $t = 0$) and slowly proceeds towards phase separation (middle row, $t = 50t_0$ and bottom row, $t = 100t_0$). From Ref. [23].
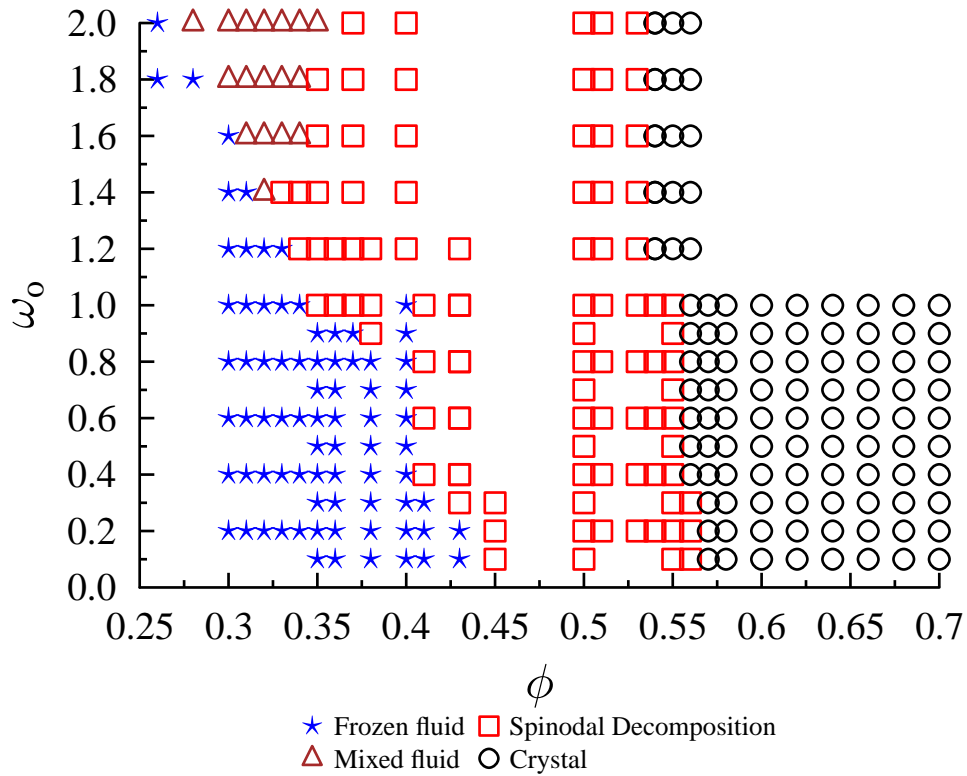
Figure B.6 Phase diagram in the ϕ-ω_0 plane at (or near) steady state for systems of $N = 16,384$ spinners, where half rotate clockwise and half rotate counterclockwise. Four phases are identified: frozen state, mixed fluid, phase separated fluid and rotating crystal phase. Each data point corresponds to one independent simulation, where we identified the prevailing steady state in the final simulation frame. Lines are drawn to separate regions where the same steady state is observed. Rotating crystals typically coexist with phase-separated fluid. The transition from mixed fluid to phase-separated fluid is smeared out, all the other transitions are sharp. From Ref. [23].
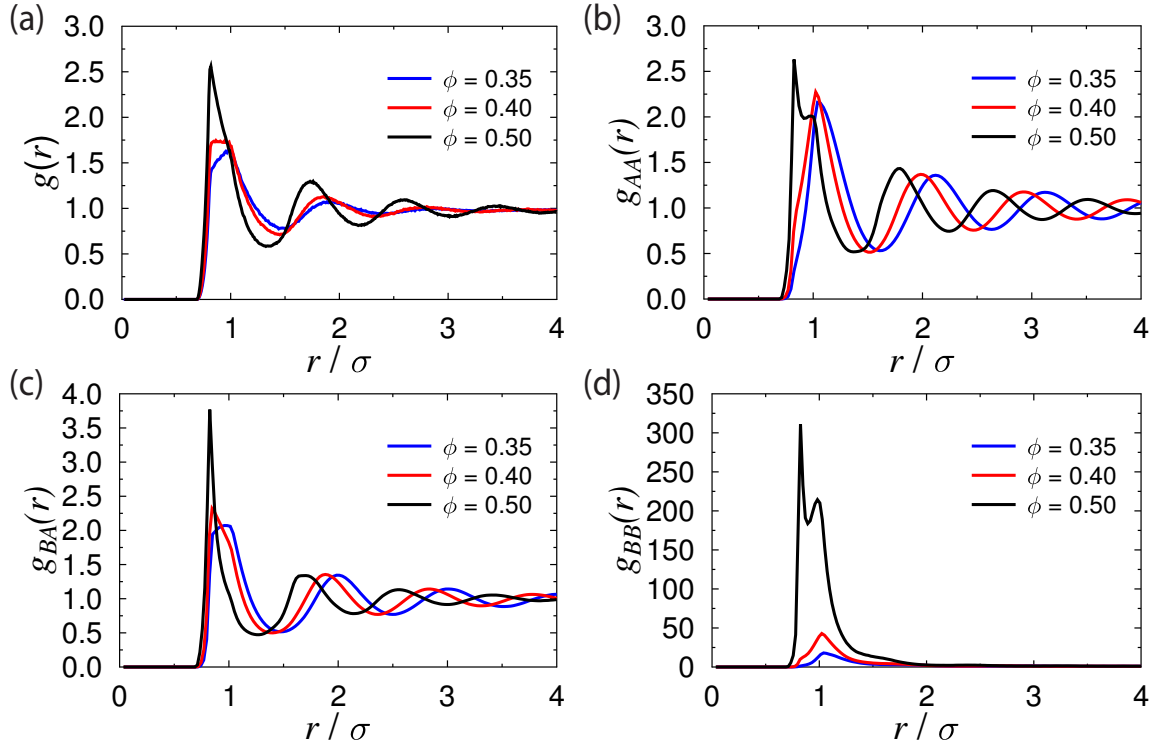
Figure B.7 Radial distribution function $g(r) \equiv \rho(r)/\rho(L/2)$ at three densities for the following systems (L is the edge length of the square simulation box): (a) $N = 100$ inactive (non-driven) particles, $\omega_0 = 0$, $T^* = 5$; (b-d) a mixture of $N_A = 98$ clockwise spinners (matrix) and $N_B = 2$ counter-clockwise spinners (intruders), $\omega_0 = 1$, $T^* = 0$. We compare correlations for matrix-matrix pairs (b), intruder-matrix pairs (c), and the intruder-intruder pair (d). Each intruder strongly prefers the vicinity of the other. Note that compared to the inactive pairs, the position of the first well of $g(r)$ the active particles shifts to higher r values at low densities. This shift happens because there is still enough space at these densities for the active gears to move apart from each other to minimize collisions. From Ref. [23].
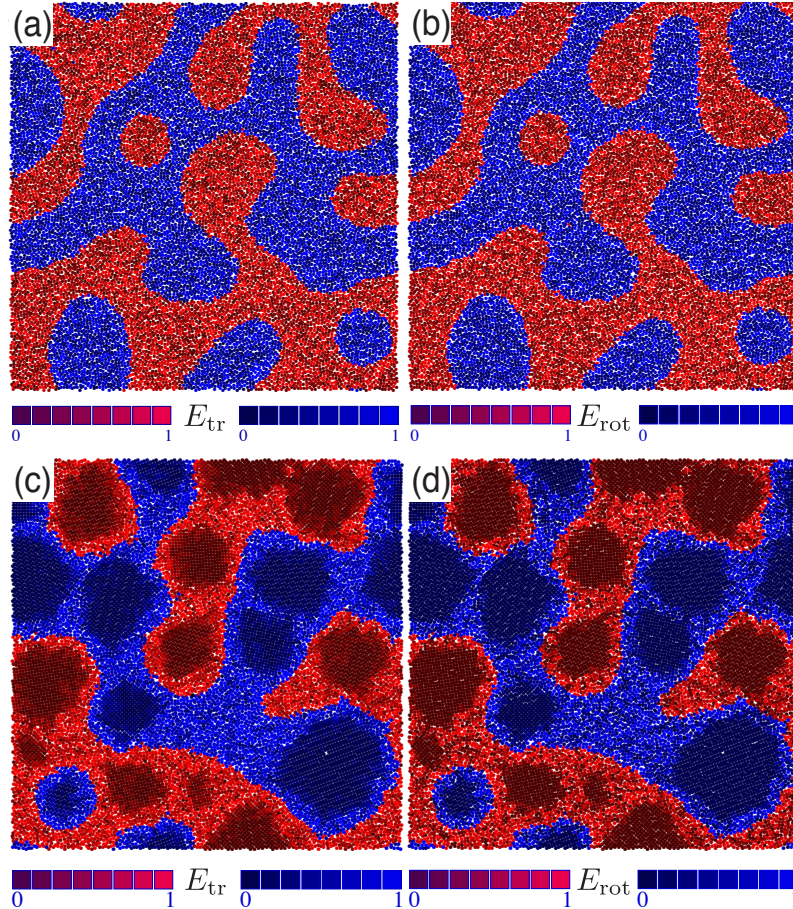
Figure B.8 Heat maps showing the kinetic energy for an even mixture of $16,384$ spinners at $\omega_0 = 1$, $T^* = 0$ and $\phi = 0.5$ (a,b) or $\phi = 0.6$ (c,d). Red and blue colors represent A and B spinners, respectively, with intensities based on the translational (E_{tr}, (a,c)) and rotational (E_{rot}, (b,d)) kinetic particle energy. Choosing the intensities linearly does not work well, because the distribution of energies (E_{rot} or E_{tr}) has a long tail. Instead, we choose intensities by first calculating the cumulative probability distribution of the energy by sorting the energy into bins. As a result, particles with the lowest (highest) kinetic energies are assigned the darkest (brightest) colors. We observe in all cases that the kinetic energy is uniform throughout each phase of the fluid, which means the interface has no significant effect. This demonstrates that the super-diffusive behavior along the interface is not the consequence of an enhanced translational and rotational velocity, but rather caused by collective directed motion. In (c,d), crystals are visible by darker colors, because particles move slower once crystallized. From Ref. [23].
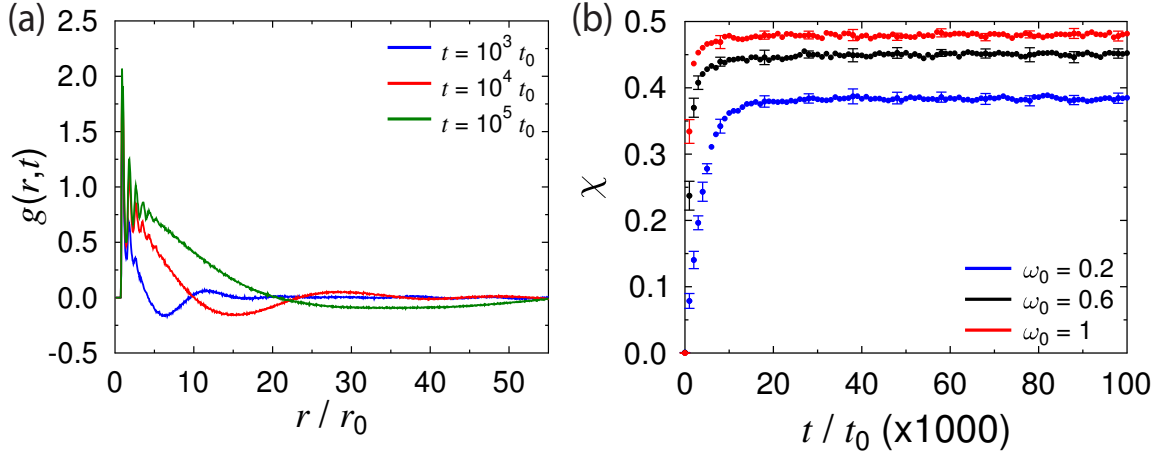
Figure B.9 (a) Radial distribution function $g(r)$ for an even mixture of 16,384 spinners at $\phi = 0.5$, $\omega_0 = 1$, $T^* = 0$, taken at three different times while the system is phase separating. We analyze the domain size growth over time (Fig. 2a) by following the first zero in $g(r)$. (b) Crystal fraction $\chi(t)$ (ratio between the number of spinners in crystals and the total number of spinners) for the same system at higher density $\phi = 0.6$ for three levels of activity. χ achieves a steady state value, demonstrating the coexistence of fluid and rotating crystals. From Ref. [23].
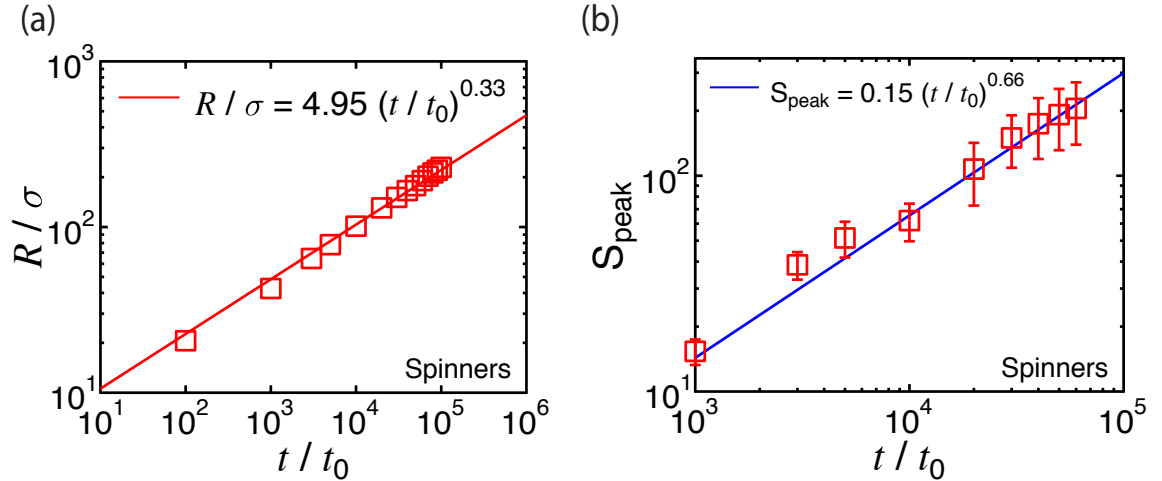
Figure B.10 The Lifshitz-Slyozov (LS) theorem predicts that in two dimensions the growth exponent of the peak of the structure factor S_{peak} is twice the exponent of growth of the domain size R in real space (see Ref. [35] of the main text). We find the LS theorem holds for our system of actively rotated spinners. (a) The growth exponent for the domain size is consistent with $1/3$. (b) The growth exponent for the peak height of the structure factor is consistent with $2/3$. Simulations are conducted with 16,384 particles at density $\phi = 0.5$. The spinners are driven with $\omega_0 = 1$ at $T^* = 0$. Note that (a) is identical to Fig. 2(a) in the main text. From Ref. [23].

Bibliography

1. Sharon C Glotzer and Michael J Solomon. Anisotropy of building blocks and their assembly into complex structures. *Nature materials*, 6(7):557–562, 2007.

2. Laura Rossi, Stefano Sacanna, William T. M. Irvine, Paul M. Chaikin, David J. Pine, and Albert P. Philipse. Cubic crystals from cubic colloids. *Soft Matter*, 7(9):4139, 2011.

3. Ching-Wen Liao, Yeh-Sheng Lin, Kaushik Chanda, Yen-Fang Song, and Michael H Huang. Formation of diverse supercrystals from self-assembly of a variety of polyhedral gold nanocrystals. *Journal of the American Chemical Society*, 135(7):2684–93, February 2013.

4. S Sacanna, W T M Irvine, P M Chaikin, and D J Pine. Lock and key colloids. *Nature*, 464(7288):575–8, March 2010.

5. Karol Miszta, Joost de Graaf, Giovanni Bertoni, Dirk Dorfs, Rosaria Brescia, Sergio Marras, Luca Ceseracciu, Roberto Cingolani, René van Roij, Marjolein Dijkstra, and Liberato Manna. Hierarchical self-assembly of suspended branched colloidal nanocrystals into superlattice structures. *Nature materials*, 10(11):872–6, November 2011.

6. Mark a. Horsch, Monica H. Lamm, and Sharon C. Glotzer. Tethered Nano Building Blocks: Toward a Conceptual Framework for Nanoparticle Self-Assembly. *Nano Letters*, 3(10):1341–1346, October 2003.

7. Z Zhang and S C Glotzer. Self-assembly of patchy particles. *Nano Letters*, 4(8):1407–1413, 2004.

8. Zhihong Nie, Daniele Fava, Eugenia Kumacheva, Shan Zou, Gilbert C Walker, and Michael Rubinstein. Self-assembly of metal-polymer analogues of amphiphilic triblock copolymers. *Nature materials*, 6(8):609–14, August 2007.

9. Fish vortex, copied from http://www.wired.com/wiredscience/2013/03/powers-of-swarms/all/, accessed date August 6 2013.

10. Ant ring of death, copied from http://xmb.stuffucanuse.com/xmb/viewthread.php?tid=7154, accessed date August 6th 2013.

11. Bacteria swarm, copied from http://chaos.utexas.edu/people/faculty/ernst-ludwig-florin/colony-growth-and-microscopic-bacterial-motion, accessed date August 6th 2013.

12. T Surrey, F Nedelec, S Leibler, and E Karsenti. Physical properties determining self-organization of motors and microtubules. *Science (New York, N.Y.)*, 292(5519):1167–71, May 2001.

13. Tamás Vicsek, András Czirók, Eshel Ben-Jacob, Inon Cohen, and Ofer Shochet. Novel Type of Phase Transition in a System of Self-Driven Particles. *Physical Review Letters*, 75(6):1226–1229, August 1995.

14. F Peruani, A Deutsch, and M Bär. Nonequilibrium clustering of self-propelled rods. *Physical Review E*, 74(3):30904, 2006.

15. Y Fily and M C Marchetti. Athermal Phase Separation of Self-Propelled Particles with No Alignment. *Physical Review Letters*, 108(23):235702, 2012.

16. Jeremie Palacci, Stefano Sacanna, Asher Preska Steinberg, David J Pine, and Paul M Chaikin. Living crystals of light-activated colloidal surfers. *Science*, 339(6122):936–940, March 2013.

17. Vijay Narayan, Sriram Ramaswamy, and Narayanan Menon. Long-Lived Giant Number Fluctuations in a Swarming Granular Nematic. *Science*, 317(5834):105–108, 2007.

18. Bartosz A Grzybowski, Howard A Stone, and George M Whitesides. Dynamic self-assembly of magnetized, millimetre-sized objects rotating at a liquid-air interface. *Nature*, 405(6790):1033–1036, 2000.

19. Jing Yan, Moses Bloom, Sung Chul Bae, Erik Luijten, and Steve Granick. Linking synchronization to self-assembly using magnetic Janus colloids. *Nature*, 491(7425):578–581, November 2012.

20. Trung Dac Nguyen, Carolyn L. Phillips, Joshua a. Anderson, and Sharon C. Glotzer. Rigid body constraints realized in massively-parallel molecular dynamics on graphics processing units. *Computer Physics Communications*, 182(11):2307–2313, November 2011.

21. Nguyen H P Nguyen, Eric Jankowski, and Sharon C Glotzer. Thermal and athermal three-dimensional swarms of self-propelled particles. *Physical Review E*, 86(1):11136, July 2012.

22. See Appendix B for movies and additional figures.

23. Nguyen H P Nguyen, Daphne Klotsa, Michael Engel, and Sharon C Glotzer. Emergent collective phenomena in a mixture of hard shapes through active rotation. *arXiv preprint arXiv:1308.2219*, 2013.

24. Iain D Couzin, Jens Krause, Richard James, Graeme D Ruxton, and Nigel R Franks. Collective Memory and Spatial Sorting in Animal Groups. *Journal of Theoretical Biology*, 218(1):1–11, 2002.

25. George M Whitesides and Bartosz Grzybowski. Self-Assembly at All Scales. *Science*, 295(5564):2418–2421, 2002.

26. Marcin Fialkowski, Kyle J M Bishop, Rafal Klajn, Stoyan K Smoukov, Christopher J Campbell, and Bartosz A Grzybowski. Principles and Implementations of Dissipative (Dynamic) Self-Assembly. *The Journal of Physical Chemistry B*, 110(6):2482–2496, 2006.

27. F X Redl, K-S Cho, C B Murray, and S O'Brien. Three-dimensional binary superlattices of magnetic nanocrystals and semiconductor quantum dots. *Nature*, 423(6943):968–71, June 2003.

28. Elena V Shevchenko, Dmitri V Talapin, Nicholas a Kotov, Stephen O'Brien, and Christopher B Murray. Structural diversity in binary nanoparticle superlattices. *Nature*, 439(7072):55–9, January 2006.

29. Angang Dong, Jun Chen, Patrick M Vora, James M Kikkawa, and Christopher B Murray. Binary nanocrystal superlattice membranes self-assembled at the liquid-air interface. *Nature*, 466(7305):474–7, July 2010.

30. Younan Xia, Yujie Xiong, Byungkwon Lim, and Sara E Skrabalak. Shape-controlled synthesis of metal nanocrystals: simple chemistry meets complex physics? *Angewandte Chemie (International ed. in English)*, 48(1):60–103, January 2009.

31. Pablo F Damasceno, Michael Engel, and Sharon C Glotzer. Predictive self-assembly of polyhedra into complex structures. *Science (New York, N.Y.)*, 337(6093):453–457, July 2012.

32. E Winfree, F Liu, L a Wenzler, and N C Seeman. Design and self-assembly of two-dimensional DNA crystals. *Nature*, 394(6693):539–44, August 1998.

33. Sung Yong Park, Abigail K R Lytton-Jean, Byeongdu Lee, Steven Weigand, George C Schatz, and Chad a Mirkin. DNA-programmable nanoparticle crystallization. *Nature*, 451(7178):553–6, January 2008.

34. Mark Horsch, Zhenli Zhang, and Sharon Glotzer. Self-Assembly of Polymer-Tethered Nanorods. *Physical Review Letters*, 95(5):056105, July 2005.

35. Mark a Horsch, Zhenli Zhang, and Sharon C Glotzer. Self-assembly of laterally-tethered nanorods. *Nano letters*, 6(11):2406–13, November 2006.

36. Elaine R. Chan, Xi Zhang, Cheng-Ying Lee, Matthew Neurock, and Sharon C. Glotzer. Simulations of Tetra-Tethered Organic/Inorganic NanocubePolymer Assemblies. *Macromolecules*, 38(14):6168–6180, July 2005.

37. Xi Zhang, Elaine R Chan, and Sharon C Glotzer. Self-assembled morphologies of monotethered polyhedral oligomeric silsesquioxane nanocubes from computer simulation. *The Journal of chemical physics*, 123(18):184718, November 2005.

38. Trung Dac Nguyen, Zhenli Zhang, and Sharon C Glotzer. Molecular simulation study of self-assembly of tethered V-shaped nanoparticles. *The Journal of chemical physics*, 129(24):244903, December 2008.

39. Salvatore Torquato. Inverse optimization techniques for targeted self-assembly. *Soft Matter*, 5(6):1157, 2009.

40. Henry Cohn and Abhinav Kumar. Algorithmic design of self-assembling structures. *Proceedings of the National Academy of Sciences of the United States of America*, 106(24):9570–5, June 2009.

41. Sahand Hormoz and Michael P Brenner. Design principles for self-assembly with short-range interactions. *Proceedings of the National Academy of Sciences of the United States of America*, 108(13):5193–8, March 2011.

42. Frank Schweitzer. *Brownian agents and active particles: collective dynamics in the natural and social sciences*. Springer, 2007.

43. Sriram Ramaswamy. The Mechanics and Statistics of Active Matter. *Annual Review of Condensed Matter Physics*, 1:323–345, 2010.

44. Tamás Vicsek and Anna Zafeiris. Collective motion. *Physics Reports*, 517(3-4):71–140, August 2012.

45. M C Marchetti, J F Joanny, S Ramaswamy, T B Liverpool, J Prost, Madan Rao, and R Aditi. Soft active matter. *arXiv preprint arXiv:1207.2929*, 2012.

46. S Ramaswamy, R Aditi Simha, and J Toner. Active nematics on a substrate: Giant number fluctuations and long-time tails. *Europhysics Letters*, 62(2):196–202, April 2003.

47. Herbert Levine, Wouter-Jan Rappel, and Inon Cohen. Self-organization in systems of self-propelled particles. *Physical Review E*, 63(1):17101, December 2000.

48. N.D. Mermin and H. Wagner. Absence of ferromagnetism or antiferromagnetism in one- or two-dimensional isotropic Heisenberg models. *Physical Review Letters*, 17(22):1133–1136, 1966.

49. J Toner and Y Tu. Long-range order in a two-dimensional dynamical XY model: How birds fly together. *Physical Review Letters*, 75(23):4326–4329, 1995.

50. Czirók András, H Eugene Stanley, and Vicsek Tamás. Spontaneously ordered motion of self-propelled particles. *Journal of Physics A: Mathematical and General*, 30(5):1375, 1997.

51. Tamás Vicsek András Czirók Mária Vicsek. Collective motion of organisms in three dimensions. *Physica A: Statistical Mechanics and its Applications*, 264(1-2):299–304, 1999.

52. A Czirók and T Vicsek. Collective behavior of interacting self-propelled particles. *Physica A: Statistical Mechanics and its Applications*, 281(1):17–29, 2000.

53. M. Aldana, V. Dossetti, C. Huepe, V. Kenkre, and H. Larralde. Phase Transitions in Systems of Self-Propelled Agents and Related Network Models. *Physical Review Letters*, 98(9):095702, March 2007.

54. Gabriel Baglietto and Ezequiel Albano. Nature of the order-disorder transition in the Vicsek model for the collective motion of self-propelled particles. *Physical Review E*, 80(5):050103, November 2009.

55. Guillaume Grégoire and Hugues Chaté. Onset of Collective and Cohesive Motion. *Physical Review Letters*, 92(2):25702, January 2004.

56. H. Chaté, F. Ginelli, and Guillaume Gregoire. Comment on Phase Transitions in Systems of Self-Propelled Agents and Related Network Models. *arXiv preprint arXiv:0711.1225*, 170(2004):5–6, 2007.

57. H. Chaté, F. Ginelli, G. Grégoire, F. Peruani, and F. Raynaud. Modeling collective motion: variations on the Vicsek model. *The European Physical Journal B*, 64(3-4):451–456, July 2008.

58. Hugues Chaté, Francesco Ginelli, and Franck Raynaud. Collective motion of self-propelled particles interacting without cohesion. *Physical Review E*, 77(4):046113, April 2008.

59. M R D'Orsogna, Y L Chuang, A L Bertozzi, and L S Chayes. Self-Propelled Particles with Soft-Core Interactions: Patterns, Stability, and Collapse. *Physical Review Letters*, 96(10):104302, March 2006.

60. U Erdmann, W Ebeling, and A S Mikhailov. Noise-induced transition from translational to rotational motion of swarms. *Physical Review E*, 71(5):51904, 2005.

61. Y Chuang, M R D'Orsogna, D Marthaler, A L Bertozzi, and L S Chayes. State transitions and the continuum limit for a 2D interacting, self-propelled particle system. *Physica D: Nonlinear Phenomena*, 232(1):33–47, 2007.

62. Jessica Strefler, Udo Erdmann, and Lutz Schimansky-Geier. Swarming in three dimensions. *Physical Review E*, 78(3):31927, September 2008.

63. Gabriel S Redner, Michael F Hagan, and Aparna Baskaran. Structure and Dynamics of a Phase-Separating Active Colloidal Fluid. *Physical Review Letters*, 110(5):55701, January 2013.

64. Gabriel S Redner, Aparna Baskaran, and Michael F Hagan. Reentrant Phase Behavior in Active Colloids with Attraction. *arXiv preprint arXiv:1303.3195*, 2013.

65. H. Wensink and H. Löwen. Aggregation of self-propelled colloidal rods near confining walls. *Physical Review E*, 78(3):031409, September 2008.

66. F Ginelli, F Peruani, M Bär, and H Chaté. Large-scale collective properties of self-propelled rods. *Physical review letters*, 104(18):184502, 2010.

67. Samuel R. McCandlish, Aparna Baskaran, and Michael F. Hagan. Spontaneous segregation of self-propelled particles with different motilities. *Soft Matter*, 8(8):2527, 2012.

68. P. C. Martin, O. Parodi, and P. S. Pershan. Unified Hydrodynamic Theory for Crystals, Liquid Crystals, and Normal Fluids. *Physical Review A*, 6(6), 1972.

69. Igor Aranson and Lev Tsimring. Pattern formation of microtubules and motors: Inelastic interaction of polar rods. *Physical Review E*, 71(5):050901, May 2005.

70. Tanniemola Liverpool. Anomalous fluctuations of active polar filaments. *Physical Review E*, 67(3):031909, March 2003.

71. J Toner and Y Tu. Flocks, herds, and schools: A quantitative theory of flocking. *Physical Review E*, 58(4):4828, 1998.

72. R. Aditi Simha and Sriram Ramaswamy. Hydrodynamic Fluctuations and Instabilities in Ordered Suspensions of Self-Propelled Particles. *Physical Review Letters*, 89(5):058101, July 2002.

73. Aparna Baskaran and M Cristina Marchetti. Hydrodynamics of self-propelled hard rods. *Physical Review E*, 77(1):11920, January 2008.

74. A Baskaran and M C Marchetti. Enhanced diffusion and ordering of self-propelled rods. *Physical Review Letters*, 101(26):268101, 2008.

75. A Baskaran and M C Marchetti. Statistical mechanics and hydrodynamics of bacterial suspensions. *Proceedings of the National Academy of Sciences*, 106(37):15567–15572, 2009.

76. Walter F Paxton, Kevin C Kistler, Christine C Olmeda, Ayusman Sen, Sarah K St. Angelo, Yanyan Cao, Thomas E Mallouk, Paul E Lammert, and Vincent H Crespi. Catalytic Nanomotors: Autonomous Movement of Striped Nanorods. *Journal of the American Chemical Society*, 126(41):13424–13431, 2004.

77. Jonathan R Howse, Richard A L Jones, Anthony J Ryan, Tim Gough, Reza Vafabakhsh, and Ramin Golestanian. Self-Motile Colloidal Particles: From Directed Propulsion to Random Walk. *Physical Review Letters*, 99(4):48102, July 2007.

78. J G Gibbs and Y.-P. Zhao. Autonomously motile catalytic nanomotors by bubble propulsion. *Applied Physics Letters*, 94(16):163104, 2009.

79. R Dreyfus, J Baudry, M L Roper, M Fermigier, H A Stone, and J Bibette. Microscopic artificial swimmers. *Nature*, 7060:862—-865, 2005.

80. Pietro Tierno, Ramin Golestanian, Ignacio Pagonabarraga, and Francesc Sagués. Controlled Swimming in Confined Fluids of Magnetically Actuated Colloidal Rotors. *Physical Review Letters*, 101(21):218304, November 2008.

81. Jared Burdick, Rawiwan Laocharoensuk, Philip M Wheat, Jonathan D Posner, and Joseph Wang. Synthetic Nanomotors in Microchannel Networks: Directional Microchip Motion and Controlled Manipulation of Cargo. *Journal of the American Chemical Society*, 130(26):8164–8165, 2008.

82. Shakuntala Sundararajan, Paul E Lammert, Andrew W Zudans, Vincent H Crespi, and Ayusman Sen. Catalytic Motors for Transport of Colloidal Cargo. *Nano Letters*, 8(5):1271–1276, 2008.

83. Ambarish Ghosh and Peer Fischer. Controlled propulsion of artificial magnetic nanostructured propellers. *Nano letters*, 9(6):2243–5, June 2009.

84. I Theurkauff, C Cottin-Bizonne, J Palacci, C Ybert, and L Bocquet. Dynamic clustering in active colloidal suspensions with chemical signaling. *Phys. Rev. Lett.*, 108(26):268303, 2012.

85. J Palacci, C Cottin-Bizonne, C Ybert, and L Bocquet. Sedimentation and effective temperature of active colloidal suspensions. *Physical Review Letters*, 105(8):88304, 2010.

86. F J Nédélec, T Surrey, a C Maggs, and S Leibler. Self-organization of microtubules and motors. *Nature*, 389(6648):305–8, September 1997.

87. Nicholas Metropolis, Arianna W. Rosenbluth, Marshall N. Rosenbluth, Augusta H. Teller, and Edward Teller. Equation of State Calculations by Fast Computing Machines. *The Journal of Chemical Physics*, 21(6):1087, 1953.

88. J.D. Bernal. The Bakerian Lecture, 1962. The Structure of Liquids. *Proceedings of the Royal Society of Longdon. Series A, Mathematical and Physical Sciences*, 280(1382):299–322, 1962.

89. B. J. Alder and T. E. Wainwright. Phase Transition for a Hard Sphere System. *The Journal of Chemical Physics*, 27(5):1208, 1957.

90. Zhenli Zhang, Aaron S Keys, Ting Chen, and Sharon C Glotzer. Self-assembly of patchy particles into diamond structures through molecular mimicry. *Langmuir*, 21(25):11547–11551, 2005.

91. Joshua A Anderson, Christian D Lorenz, and Alex Travesset. General purpose molecular dynamics simulations fully implemented on graphics processing units. *J. Comp. Phys.*, 227(10):5342–5359, May 2008.

92. Highly Optimized Object-oriented Many-particle Dynamics. *http://codeblue.umich.edu/hoomd-blue/*.

93. Albert Einstein. *Investigations on the Theory of the Brownian Movement*. DoverPublications. com, 1956.

94. A P Philipse. Notes on Brownian Motion. Technical report, 2011.

95. A C Braka and D M Heyes. Algorithms for Brownian dynamics computer simulations: multivariable case. *Physical review. E, Statistical physics, plasmas, fluids, and related interdisciplinary topics*, 60(2):2381–7, August 1999.

96. Steve Plimpton. Fast parallel Algorithms for short-range molecular dynamics. *Journal of computational physics*, (117):1–19, 1995.

97. John Toner, Yuhai Tu, and Sriram Ramaswamy. Hydrodynamics and phases of flocks. *Annals of Physics*, 318(1):170–244, 2005.

98. S Hubbard, P Babak, S T Sigurdsson, and K G Magnússon. A model of the formation of fish schools and migrations of fish. *Ecological Modelling*, 174(4):359–374, 2004.

99. S T Chang, V N Paunov, D N Petsev, and O D Velev. Remotely powered self-propelling particles and micropumps based on miniature diodes. *Nature materials*, 6(3):235–240, 2007.

100. S Mishra, A Baskaran, and M C Marchetti. Fluctuations and pattern formation in self-propelled particles. *Physical Review E*, 81(6):61916, 2010.

101. A P Chetverikov, W Ebeling, and M G Velarde. Thermodynamics and phase transitions in dissipative and active Morse chains. *The European Physical Journal B-Condensed Matter and Complex Systems*, 44(4):509–519, 2005.

102. F Schweitzer, W Ebeling, and B Tilch. Statistical mechanics of canonical-dissipative systems and applications to swarm dynamics. *Physical Review E*, 64(2):21110, 2001.

103. Jihad R Touma, Amer Shreim, and Leonid I Klushin. Self-organization in two-dimensional swarms. *Physical Review E*, 81(6):66106, June 2010.

104. Y L Chuang, Y R Huang, M R D'Orsogna, and A L Bertozzi. Multi-vehicle flocking: scalability of cooperative control algorithms using pairwise potentials. In *Robotics and Automation, 2007 IEEE International Conference on*, pages 2292–2299. IEEE, 2007.

105. P Ogren, E Fiorelli, and N E Leonard. Cooperative control of mobile sensor networks: Adaptive gradient climbing in a distributed environment. *Automatic Control, IEEE Transactions on*, 49(8):1292–1302, 2004.

106. J M Deutch and I Oppenheim. Molecular theory of Brownian motion for several particles. *The Journal of Chemical Physics*, 54:3547, 1971.

107. L Verlet. Computer "experiments" on classical fluids. I. Thermodynamical properties of Lennard-Jones molecules. *Physical Review*, 159(1):98, 1967.

108. S J Plimpton. http://lammps.sandia.gov/. 2009.

109. Y Shi, L Huang, and D W Brenner. Computational study of nanometer-scale self-propulsion enabled by asymmetric chemical catalysis. *The Journal of chemical physics*, 131:14705, 2009.

110. Julian Bialké, Thomas Speck, and Hartmut Löwen. Crystallization in a Dense Suspension of Self-Propelled Particles. *Physical Review Letters*, 108(16):168301, April 2012.

111. H H Wensink, V Kantsler, R E Goldstein, and J Dunkel. Controlling active self-assembly through broken particle symmetries. *arXiv preprint arXiv:1306.0709*, 2013.

112. J Tailleur and M E Cates. Statistical mechanics of interacting run-and-tumble bacteria. *Phys. Rev. Lett.*, 100(21):218103, 2008.

113. M E Cates, J Tailleur, and United Kingdom. When are active Brownian particles and run-and-tumble particles equivalent ? Consequences for motility-induced phase separation. *Europhysics Letters*, 101(2):1–7, 2013.

114. Joakim Stenhammar, Adriano Tiribocchi, Rosalind J Allen, Davide Marenduzzo, and Michael E Cates. A continuum theory of phase separation kinetics for active Brownian particles. *Physical Review Letters*, 111(14):145702, 2013.

115. Ivo Buttinoni, Julian Bialké, Felix Kümmel, Hartmut Löwen, Clemens Bechinger, and Thomas Speck. Dynamical Clustering and Phase Separation in Suspensions of Self-Propelled Colloidal Particles. *Physical Review Letters*, 110(23):238301, June 2013.

116. A Kudrolli, G Lumay, D Volfson, and L S Tsimring. Swarming and swirling in self-propelled polar granular rods. *Physical Review Letters*, 100(5):58001, 2008.

117. Klaus Roeller, James P D Clewett, R M Bowley, Stephan Herminghaus, and Michael R Swift. Liquid-Gas Phase Separation in Confined Vibrated Dry Granular Matter. *Physical Review Letters*, 107(4):48002, July 2011.

118. Bartosz A Grzybowski and George M Whitesides. Dynamic aggregation of chiral spinners. *Science*, 296(5568):718–721, April 2002.

119. David G Grier. Optical tweezers in colloid and interface science. *Current opinion in colloid \& interface science*, 2(3):264–270, June 1997.

120. Jeffrey R Moffitt, Yann R Chemla, Steven B Smith, and Carlos Bustamante. Recent advances in optical tweezers. *Annual Reviews Biochemistry*, 77:205–228, January 2008.

121. Alejandro V Arzola, Martin Šiler, Oto Brzobohatý, Petr Jákl, and Pavel Zemánek. Rotation of microscopic discs by the angular momentum of light. *SPIE Proceedings*, 8458:84582U, October 2012.

122. Knut Drescher, Kyriacos Leptos, Idan Tuval, Takuji Ishikawa, Timothy Pedley, and Raymond Goldstein. Dancing Volvox: Hydrodynamic Bound States of Swimming Algae. *Physical Review Letters*, 102(16):168101, April 2009.

123. I H Riedel, K Kruse, and J Howard. A self-organized vortex array of hydrodynamically entrained sperm cells. *Science*, 309(5732):300, 2005.

124. Felix Kümmel, Borge ten Hagen, Raphael Wittkowski, Ivo Buttinoni, Ralf Eichhorn, Giovanni Volpe, Hartmut Löwen, and Clemens Bechinger. Circular Motion of Asymmetric Self-Propelling Particles. *Physical Review Letters*, 110(19):198302, May 2013.

125. Yaouen Fily, Aparna Baskaran, and M. Cristina Marchetti. Cooperative self-propulsion of active and passive rotors. *Soft Matter*, 8(10):3002, 2012.

126. Nariya Uchida and Ramin Golestanian. Synchronization and Collective Dynamics in a Carpet of Microfluidic Rotors. *Physical Review Letters*, 104(17):178103, April 2010.

127. A Kaiser and H Löwen. Vortex arrays as emergent collective phenomena for circle swimmers. *Physical Review E*, 87(3):32712, March 2013.

128. John D Weeks and David Chandler. Role of Repulsive Forces in Determining the Equilibrium Structure of Simple Liquids. *Journal of Chemical Physics*, 54(12):5237, 1971.

129. Knut Drescher, Jörn Dunkel, Luis H Cisneros, Sujoy Ganguly, and Raymond E Goldstein. Fluid dynamics and noise in bacterial cell-cell and cell-surface scattering. *Proceedings of the National Academy of Sciences of the United States of America*, 108(27):10940–10945, July 2011.

130. Haye Hinrichsen. Non-equilibrium critical phenomena and phase transitions into absorbing states. *Advances in physics*, 49(7):815–958, November 2000.

131. Laurent Corté, P M Chaikin, J P Gollub, and D J Pine. Random organization in periodically driven systems. *Nature Physics*, 4(5):420–424, March 2008.

132. Volker Schaller, Christoph A Weber, Benjamin Hammerich, Erwin Frey, and Andreas R Bausch. Frozen steady states in active systems. *Proceedings of the National Academy of Sciences of the United States of America*, 108(48):19183–19188, November 2011.

133. J Schwarz-Linek, C Valeriani, A Cacciuto, M E Cates, D Marenduzzo, A N Morozov, and W C K Poon. Phase separation and rotor self-assembly in active particle suspensions. *Proceedings of the National Academy of Sciences of the United States of America*, 109(11):4052–4057, March 2012.

134. Andreas M Menzel and Hartmut Löwen. Traveling and Resting Crystals in Active Systems. *Physical Review Letters*, 110(5):55702, February 2013.

135. I. M. Lifshitz and V. V. Slyozov. The kinetics of precipitation from supersaturated solid solutions. *Journal of Physics and Chemistry of Solids*, 19(1):35–50, 1961.

136. S W Koch, Rashmi C Desai, and Farid F Abraham. Dynamics of phase separation in two-dimensional fluids: Spinodal decomposition. *Physical Review A*, 27(4):2152–2167, 1983.

137. E Velasco S Toxvaerd. Computer Simulation of Phase Separation in a Two-Dimensional Binary Fluid Mixture. *Physical Review Letters*, 71(3):388–391, 1993.

138. Sharon C Glotzer, Edmund A Di Marzio, and M Muthukumar. Reaction-Controlled Morphology of Phase-Separating Mixtures. *Physical Review Letters*, 74(11), 1995.

139. Q.-X. Liu, A Doelman, V Rottschafer, M de Jager, P M J Herman, M Rietkerk, and J van de Koppel. Phase separation explains a new class of self-organized spatial patterns in ecological systems. *Proceedings of the National Academy of Sciences of the United States of America*, 110(29):11905, July 2013.

140. B. Smit and D. Frenkel. Vaporliquid equilibria of the two-dimensional Lennard-Jones fluid(s). *The Journal of Chemical Physics*, 94(8):5663, 1991.

141. L Onsager. Crystal statistics I A two-dimensional model with an order-disorder transition. *Physical Review*, 65:117–149, 1944.

142. Walter Kob, Claudio Donati, Steven J. Plimpton, Peter H. Poole, and Sharon C. Glotzer. Dynamical Heterogeneities in a Supercooled Lennard-Jones Liquid. *Physical Review Letters*, 79(15):2827–2830, October 1997.

143. Claudio Donati, Jack F Douglas, Walter Kob, Steven J Plimpton, Peter H Poole, and Sharon C Glotzer. Stringlike Cooperative Motion in a Supercooled Liquid. *Phys. Rev. Lett.*, 80(11):2338–2341, March 1998.

144. Vinothan N Manoharan, Mark T Elsesser, and David J Pine. Dense packing and symmetry in small clusters of microspheres. *Science*, 301(5632):483–487, 2003.

145. Itai Cohen, Thomas Mason, and David Weitz. Shear-Induced Configurations of Confined Colloidal Suspensions. *Physical Review Letters*, 93(4):046001, July 2004.

146. Yilong Han and David Grier. Confinement-Induced Colloidal Attractions in Equilibrium. *Physical Review Letters*, 91(3):038302, July 2003.

147. William T M Irvine, Mark J Bowick, and Paul M Chaikin. Fractionalization of interstitials in curved colloidal crystals. *Nature materials*, 11(11):948–51, November 2012.

148. J a Moreno-Razo, E J Sambriski, N L Abbott, J P Hernández-Ortiz, and J J de Pablo. Liquid-crystal-mediated self-assembly at nanodroplet interfaces. *Nature*, 485(7396):86–9, May 2012.

149. Joy Y Cheng, Anne M Mayes, and Caroline a Ross. Nanostructure engineering by templated self-assembly of block copolymers. *Nature materials*, 3(11):823–8, November 2004.

150. Peng Chi, Zheng Wang, Baohui Li, and An-Chang Shi. Soft confinement-induced morphologies of diblock copolymers. *Langmuir : the ACS journal of surfaces and colloids*, 27(18):11683–9, September 2011.

151. An-Chang Shi and Baohui Li. Self-assembly of diblock copolymers under confinement. *Soft Matter*, 9(5):1398, 2013.

152. Richard M. Jendrejack, David C. Schwartz, Michael D. Graham, and Juan J. de Pablo. Effect of confinement on DNA dynamics in microfluidic devices. *The Journal of Chemical Physics*, 119(2):1165, 2003.

153. Juan P. Hernandez-Ortiz, Christopher G. Stoltz, and Michael D. Graham. Transport and Collective Dynamics in Suspensions of Confined Swimming Particles. *Physical Review Letters*, 95(20):204501, November 2005.

154. Andrey Sokolov, Igor Aranson, John Kessler, and Raymond Goldstein. Concentration Dependence of the Collective Dynamics of Swimming Bacteria. *Physical Review Letters*, 98(15):158102, April 2007.

155. Juan P Hernandez-Ortiz, Patrick T Underhill, and Michael D Graham. Dynamics of confined suspensions of swimming particles. *Journal of physics. Condensed matter : an Institute of Physics journal*, 21(20):204107, May 2009.

156. Allison Berke, Linda Turner, Howard Berg, and Eric Lauga. Hydrodynamic Attraction of Swimming Microorganisms by Surfaces. *Physical Review Letters*, 101(3):038102, July 2008.

157. C Casagrande and M Veyssié. Janus beadsrealization and 1st observation of interfacial properties. *CR Acad. Sci*, 306:1423–1425, 1988.

158. Ines C Pons-Siepermann and Sharon C Glotzer. Design of patchy particles using quaternary self-assembled monolayers. *ACS nano*, 6(5):3919–3924, 2012.

159. Ran Ni, Martien A. Cohen Stuart, Marjolein Dijkstra, and Peter G. Bolhuis. Crystallizing hard-sphere glasses by doping with active particles. *arXiv preprint arXiv:1310.7490*, October 2013.

160. Ran Ni, Martien a Cohen Stuart, and Marjolein Dijkstra. Pushing the glass transition towards random close packing using self-propelled hard spheres. *Nature communications*, 4:2704, October 2013.